POLITECNICO DI TORINO

Master degree course in Communications and Computer Networks Engineering

Master Degree Thesis

Adaptive Modulation Schemes for High-Capacity Free-Space Optics Communications

POLITECNICO DI TORINO

Supervisors
Prof. Andrea Carena

Candidates
Federico Rocco

External Tutor at Instituto de Telecomunicações (IT)
Fernando Pedro Pereira Guiomar, PhD

October, 2019

Summary

The eager for higher data rates and link capacity keep increasing in recent years.

Most of today's used wireless connections will have difficulty to face future demands because of their intrinsic limitations and there is the need for alternative solutions.

Free-Space Optics (FSO) can insert in this scenario as a possible high-capacity fixed wireless optical transmission.

Although many works, mainly theoretical, have been done, demonstration of FSO as an high capacity link still lack of further practical validations.

The goal of this thesis is to prove a reliable FSO outdoor communication able to resist atmospheric impairments and guaranteeing transmission rates of more than 400 Gbps in a 55 m link thanks to the joint use of Probabilistic Constellation Shaping (PCS) and channel predictors.

Acknowledgements

First of all, I would like to thank my parents for giving me the opportunity to meet the future head-on, to my brother Emanuele and all my family, for raising me up and making me become the man I am now.

Many thanks to the whole "Instituto de Telecomunicações" (IT) in Aveiro for accepting me and giving me the chance to develop my thesis and to all the staff and members for the help; among them, I personally want to thank Abel-Lorences Riesgo and prof. Paulo Monteiro for their everyday assistance, Ms. Sandra Corujo for her operativity and patience and Daniel Ranzal Albergaria for his huge support to this work, both practical and emotional (and especially for all the "alignment nights" we shared in IT).

A lot of gratitude goes to my external supervisor in IT, Fernando Guiomar, PhD, the mind behind this thesis, a person whose remarkable passion and attitude towards scientific world should serve as an example for many people. Thanks for all the kindness and opportunities you gave me, dignifying my stay in Aveiro and, most importantly, my future.

Thanks to professor Carena, for believing in me, supervising my thesis and making my period abroad occur. In this regard, a special thank you to Ann Margareth Rosa Brusin firstly for the support during our studies and then for the help, advices and support in reaching Aveiro and developing this thesis.

Many thanks to my Sarah, always supportive and patient. Thank you for your love, for the daily growth we confront together and all the lived experiences.

I want to personally express my gratitude to my "non-blooded" family, the "Emilio Tauro", the "Iper", the "Top Club" and all the "Chierese" friends for all the adventures we face together everyday.

Thanks to the Italians in Aveiro, my flatmates in particular, for making my experience abroad unforgettable and to local Renatinho for all the help and altruism.

Thanks to all my university friends and colleagues for the help, the laughters and the crying we had together.

In the end, thanks to all the people, past, present and future, as I think anyone, positively or negatively, helps everyday in shaping our soul.

Contents

List of Figures

List of Tables

Acronyms

3GPP Third Generation Partnership Project

AIR Achievable Information Rate

ASE Amplified Spontaneous Emission

ATP Acquisition, Tracking and Pointing

AWG Arbitrary Waveform Generator

BER Bit Error Rate

C-RAN Cloud Radio Access Network

CapEx Capital Expenditure

CCDM Constant Composition Distribution Matcher

CMA Constant Modulus Algorithm

DM Distribution Matcher

DSP Digital Signal Processing

ECL External Cavity Laser

EDFA Erbium Doped Fibers

EVM Error-Vector Magnitude

FEC Forward Error Correction

$\mathbf{FEC}_{\mathrm{oh}}$ FEC overhead

FIR Finite Impulse Response

FOV Field-of-View

FSO Free-Space Optics

H Entropy

IQ In-phase and Quadrature

LMS Least-Mean Square

LOS Line-of-sight

LPF Low Pass Filter

LUT Look-Up Table

MA Moving Average

MIMO Multiple Input Multiple Output

MSE Mean Square Error

NGMI Normalized Generalized Mutual Information

NIR Near infra-red

PCS Probabilistic Constellation Shaping

QAM Quadrature Amplitude Modulations

QoS Quality of Service

QPSK Quadrature Phase Shift Keying

RF Radio Frequency

RRC Raise Root Cosine

SNR Signal-to-Noise-Ratio

UAV Unmanned Aerial Vehicle

URLLC Ultra Reliable Low Latency Communication

VOA Variable Optical Attenuator

List of Symbols

C_1 constant to weight the feedback action of the error term in the MA-feedback formula

C_2 constant to weight the differential action of the error term in the MA-feedback algorithms formulas

δ proportional derivative term for the MA-feedback algorithms

ϵ error term for the MA-feedback algorithms

$\mathbf{M}$ constellation size

$\mathbf{NGMI}_{\mathrm{th}}$ NGMI threshold

$\mathbf{N}_{\mathrm{Pol}}$ number of polarizations

$\mathbf{R}_{\mathrm{b}}$ achievable bit rate

$\mathbf{R}_{\mathrm{FEC}}$ FEC overhead ratio

$\mathbf{R}_{\mathrm{pil}}$ pilot rate

$\mathbf{R}_{\mathrm{s}}$ gross symbol rate

$\mathbf{T}_{\mathrm{s}}$ fso channel power acquisition sampling period

Chapter 1

Introduction

1.1 Thesis structure

- Chapter 1 : This chapter presents the state of the art of FSO and PCS.
- Chapter 2 : A description of the outdoor FSO experimental setup for collecting power measurements is provided. Then, power measurements are used to analyze the link loss, develop channel predictors and investigate weather profiling.
- Chapter 3 : A simulated high capacity transmission is performed in order to demonstrate the advantage of using an adaptive transmission scheme with respect to a non-adaptive one.
- Chapter 4 : A three hours real time outdoor free space optics transmission is tested for both adaptive and non-adaptive modulated transmissions. Rain resilience and further proof of adaptive transmission gains are shown.
- Chapter 5 : Conclusions and future works are presented.

1.2 Contributions

Working on this thesis lead to some important outcomes such as :

- Paper published as co-author presented in Lisbon in June,26-28 2019 at the ConfTele conference entitled "Characterization and Modeling of Link Loss for an Outdoor Free-Space Optics Transmission System"
- Presentation of the paper "High-Capacity and Rain-Resilient Free-Space Optics Link Enabled by Time-Adaptive Probabilistic Shaping" in Dublin at the ECOC forum in September, 24$^{\text{th}}$ 2019.
- The possibility of a journal paper adapted on this thesis is under investigation.

1.3 State of the art

1.3.1 Free-Space Optics

The use of light to transmit information wirelessly is as old as human history, from beacon fires of first humans passing by more sophisticated systems such as the heliograph and the photophone at the end of 19th and the beginning of the 20th century [1] until modern era devices such as the remote control. Anyway, optical wireless communication is re-gaining nowadays more and more attention in every field, from research to industry levels, because of enhancements in optical communications in the last years.

The increase in data demand is the obvious trend due to more and more connected users, devices and multimedia applications, especially in the last decade, requiring a lot of throughput both for download and upload traffic, with the latter dramatically increasing during the last years because of social media. Internet traffic is growing year after year because of its integration level of different services, from voice over IP (VoIP) to multimedia streams. A perfect predictive scenario is provided by Cisco in [2] where networking IP traffic growth is predicted to have an increase of 20 to 30 % for the period 2017-2022.

Optical wired networks, can provide huge bandwidth (GHz), transmission speed and very low Bit Error Rate (BER) and networking companies are seeking to exploit them as much as they can in order to have an almost fully optical physical layer, continuing to increase their capacity with new modulation formats, new amplification systems and reducing their losses. Passive optical networks and fiber-to-the-building are now reality and in some cases is possible to have fiber connected directly to the user (fiber-to-the-home). Unfortunately, as any kind of wired technology, the deployment is neither simple nor cheap especially in urban area where installation requires drilling, raising the CapEx expenses to very high levels. Fiber, in particular, can also be easily damaged and in certain areas the displacement is even impossible. Nevertheless, they are the obliged solution for very high speed connections.

Radio wireless networks have the great peculiarity of allowing mobility and good connectivity to many users at the same time but they are falling short of usable bandwidth as the worldwide used spectrum is very crowded. In fact, most of wireless technology transmits in the same licensed 0-3 GHz band, thus the available bandwidth is very limited (MHz) resulting in low achievable bit rates ; anyway, the new mobile generation 5G is looking forward to exploit unlicensed high frequency bands such as the mmWave ones, because of the huge amount of available bandwidth that will help in matching requirements for high bit rates, ultra low latency and QoS demands. Good results can already be shown in frequencies up to 6 GHz (IEEE 802.11p is able to guarantee short range Mbps connection in the 5.85-5.92 GHz band).

MIMO technologies can either be used to help pushing the bit rates up to the Gbps or be exploited for massive Internet of Things applications, speaking of which is going to be a serious scenario to consider as the predicted number of connected devices for the 2020 is ~30 billion [3] . In any case, after 6 GHz no more than few cm can be guaranteed in terms of link distance; mmWave and THz wave transmissions' intrinsic technological limitations and high development costs make them difficult to be implemented.

FSO consists in launching an optical beam wirelessly from a transmitter to a receiver. Therefore it may be the perfect convergence point between wired optical and radio wireless technologies as is able to solve their issues offering ease to deploy solutions as well as a big uncrowded and unlicensed spectrum; in fact it has the ability to provide strong signal in the unlicensed THz spectrum domain both indoor and outdoor. This, along with the fact that with a very simple low cost setup is possible to obtain a quite stable link, let next cellular generation manufacturers to grow their interest towards it as a appetible solution for the fronthaul deployment as well as metropolitan area network (MAN) extension, local area network (LAN)-to-LAN connectivity, last mile access, fiber back-up and many others. Back to the 5G, the free space optics is being considered as valid solution for modern C-RAN networks as well as in 5G+ vertical fronthaul scenario in which the C-RAN can be enhanced using UAV of various types to transport point to point signal from access to core network where the focus is in dense small cells depolyments [4] (Facebook's internet.org and Google's Loon project are already working on similar topic [5], Fig.12).

FSO increasing involvement in the fronthaul for next mobile generations is represented in Fig. 1.1.

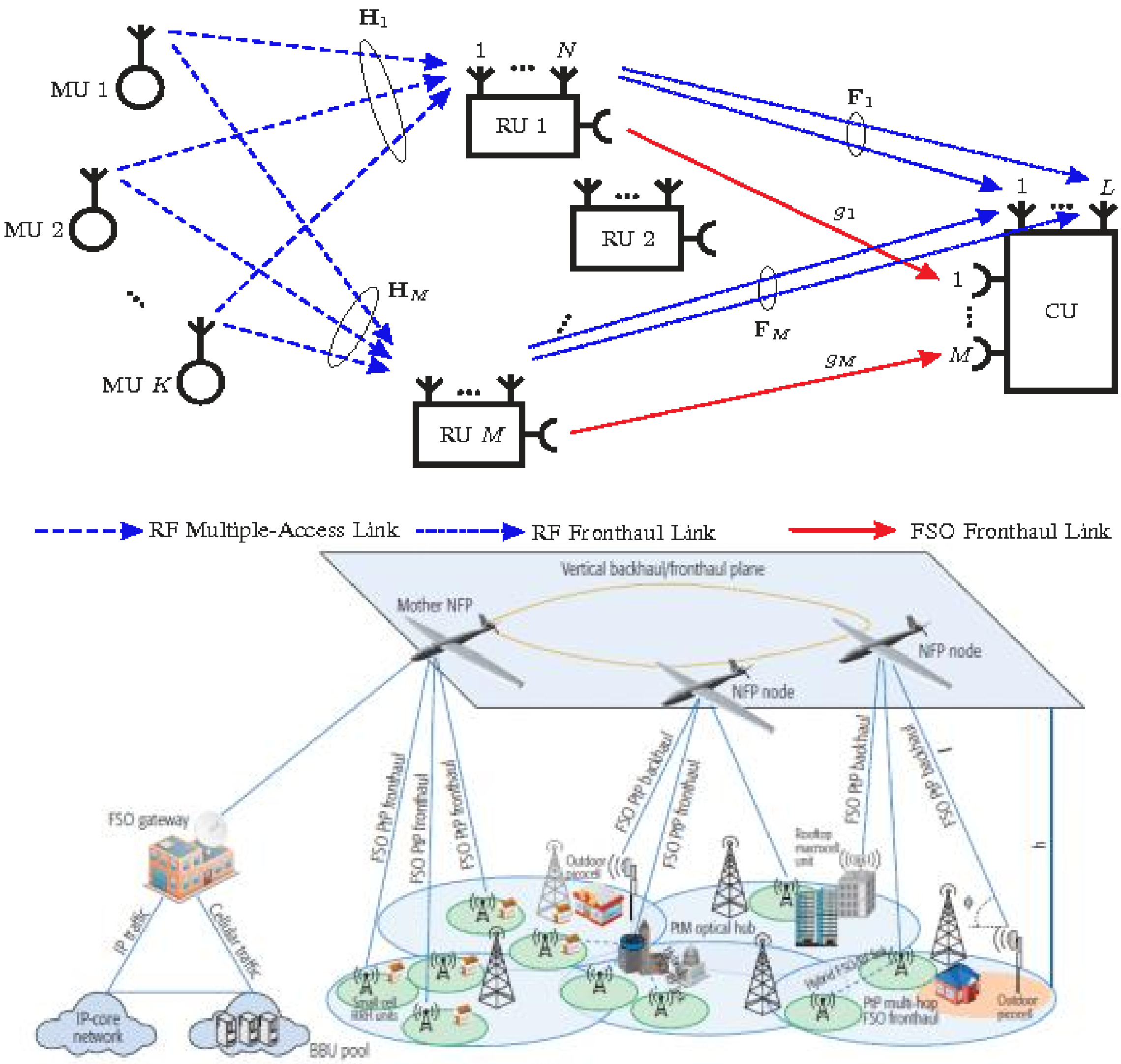

Figure 1.1: FSO integration in fronthaul deployments for next cellular generations : 5G C-Ran fronthaul with FSO integration (upper, from [6]) and 5G+ FSO for vertical fronthaul with UAV (bottom, from [4])

It can also be used as an alternative or as a support for RF communications. In Table 1.1 is reported a recap, in part adapted from [7], that compares our study case scenario against what can be obtained by using a Radio Frequency (RF) equipment. Both technologies have their advantages and limitations and their joint work will be better discussed in chapter 5.

There exist many types of FSO communication systems and in [8] a very specific classifications is made based on : the coverage type (point coverage or cellular coverage when a transmission is respectively intended for a single receiver or multiple receivers), Line-of-sight (LOS) or non-line-of-sight link (NLOS), the mobility (referring to a fixed or mobile link), link distance (from ultra short, e.g. chip-to-chip communication, to ultra long, e.g. deep space connections) and indoor/outdoor transmission. Following the same classification, the work of this thesis entirely focuses on a point coverage, LOS, fixed, medium range outdoor link. The LOS characteristic ensures a secure way of transmitting information with respect to normal radio

Table 1.1: Comparison of typical implemented terrestrial free space optics and radio frequency transmission systems

	FSO	**RF**
Bandwidth	GHz	MHz
Throughput	Gbps	Mbps
Mobility	Low	High
Stability	Low	High
Central frequency	THz	GHz
Distance	m	km
Spectrum	Unlicensed	Licensed
Interference	Low	High
Connection	LOS (Secure)	Broadband (Not secure)
Overall costs	Low	High
Human security	Frequency dependent	Frequency dependent
Power consumption	Low	High

broadband transmissions because signal can't be eavesdropped and most importantly the interference with RF systems is automatically avoided in critical scenario such as hospitals or aircrafts.

Other FSO systems, out of the scope from this study, that is worth mentioning and that are in part presented in [9] are:

- Indoor communications
- Inter-chip communication
- Television
- Underwater communications
- Wearable technologies
- Vehicular
- Medical applications
- Inter-satellite and deep space communication
- Security and surveillance

A simple scheme showing some possible usages of FSO is depicted in Fig. 1.2.

Whenever talking about optical communications, the transmitting wavelength is a critical parameter to choose for. Depending on the type of communication, different bands can be used. For example, visual light (VL) is chosen for indoor transmissions, while underwater communications work in Near infra-red (NIR) range. NIR is also the one used in this work (in fact the focus is on a 1550 nm transmission) and in general in terrestrial FSO systems because of its many advantages : first of all it is the best window to counteract atmospheric absorption , then is the same window used in modern fiber based networks (so the same hardware can be re-used to feed the fso system) and lastly is also the one in which optical amplification is performed since Erbium Doped Fibers (EDFA) work in 1520-1600nm range.

1550nm is a good solution also in terms of human security; in fact whenever talking about optical sources, safety concerns need to be taken into account. At these wavelengths, much more power can be transmitted at 1520–1600 nm than the one that can be transmitted at 780–850 nm for the same eye safety classification [9]. There are a lot of institutions providing standards about human safety because optical beams can be a major treat especially for skin and eye with the latter being more severe because of the retina ability to focus light within a certain range [10]. Graphs in Fig. 1.3 show the "1550 nm benefits".

Focusing on terrestrial FSO transmissions, many works still need to be done as they are affected by many impairments. The transmission range is limited because of its high dependency on atmospherical conditions; in fact with fog the loss can be theoretically more than 200 dB/km [4, 10] and even worse with snow [11]. Rain, on the contrary, shouldn't affect a FSO link that much and a practical demonstration of this is going to be presented in this thesis. Indeed rain attenuation is more gentle because the transmission wavelength (1,55 μm) is way smaller than rain droplets diameter (100 μm) while fog particles, instead, are of the same order of magnitude and that's the reason why FSO transmission is so affected. Anyway, other underrated elements such as pollution,dust,smoke ecc. typical of urban environments must be taken into account as they as well absorb transmitted light causing an attenuation of the optical power.

Another impairment strictly related to the transmitter-receiver distance is the geometric loss that is due to the divergence of optical transmitted beam when propagating through the atmosphere resulting in lower received power at the receiving front end. A good help to overcome this problem can be use tracking and pointing mechanisms. Since these kind of systems may apport benefits to the setup that is going to be studied, this point will be better explored in the conclusions section.

Other adverse effects in the atmospheric channel are scintillation and scattering [12]. Scintillation as well depends on the range of transmission and is caused by thermally induced changes in the index of

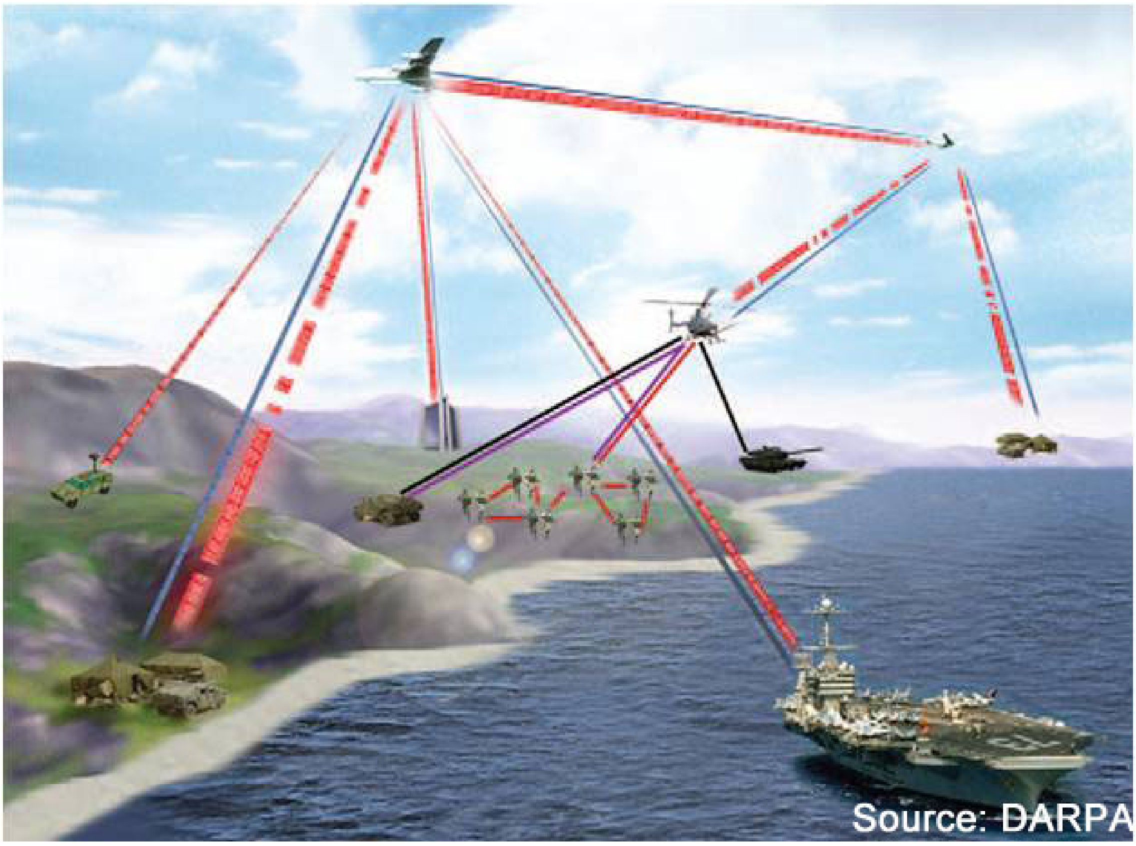

Figure 1.2: Possible free space optics applications (in red). By US Federal Government Employee - DARPA ORCA Concept Art, Public Domain, https://commons.wikimedia.org/w/index.php?curid=36430756

refraction of the air along the beam transmit path and as a result, the received irradiance at receiver will randomly fluctuate with deflection of portions of the light beam into and out of the transmit path. Scattering, instead, is due to irregularities in propagation medium. Its effect cause beam wandering,i.e. a random path followed by the beam when propagating.

Base motion is another important concept that should be taken into account. As presented in [10] there can be three different types of base motion and any of them will result in signal sway at receiver side . Our setup is not mounted on top of a building so the main concerns are about high frequency base motions meaning motions caused by environment machinery , human activity and wind. Some solutions to these problems are suggested in [13].

Even if some works have been made, mobility and broadband features are still limited because of way too difficult implementations issues as can be extrapolated from [8]. The usage of mainly LOS links results in highly directional and narrow beams transmissions and a temporal signal interruption by anything interfering with the beam can always occur.

Other minor impairments should be taken into account as for example thermal expansion and direct intense sunlight which can produce interference because of background radiation. In the studied system , the sunlight (direct, reflected or scattered) is a constant presence as it normally is for an outdoor FSO link. Its effect can be a reduced SNR and effective receiver sensitivity [14].

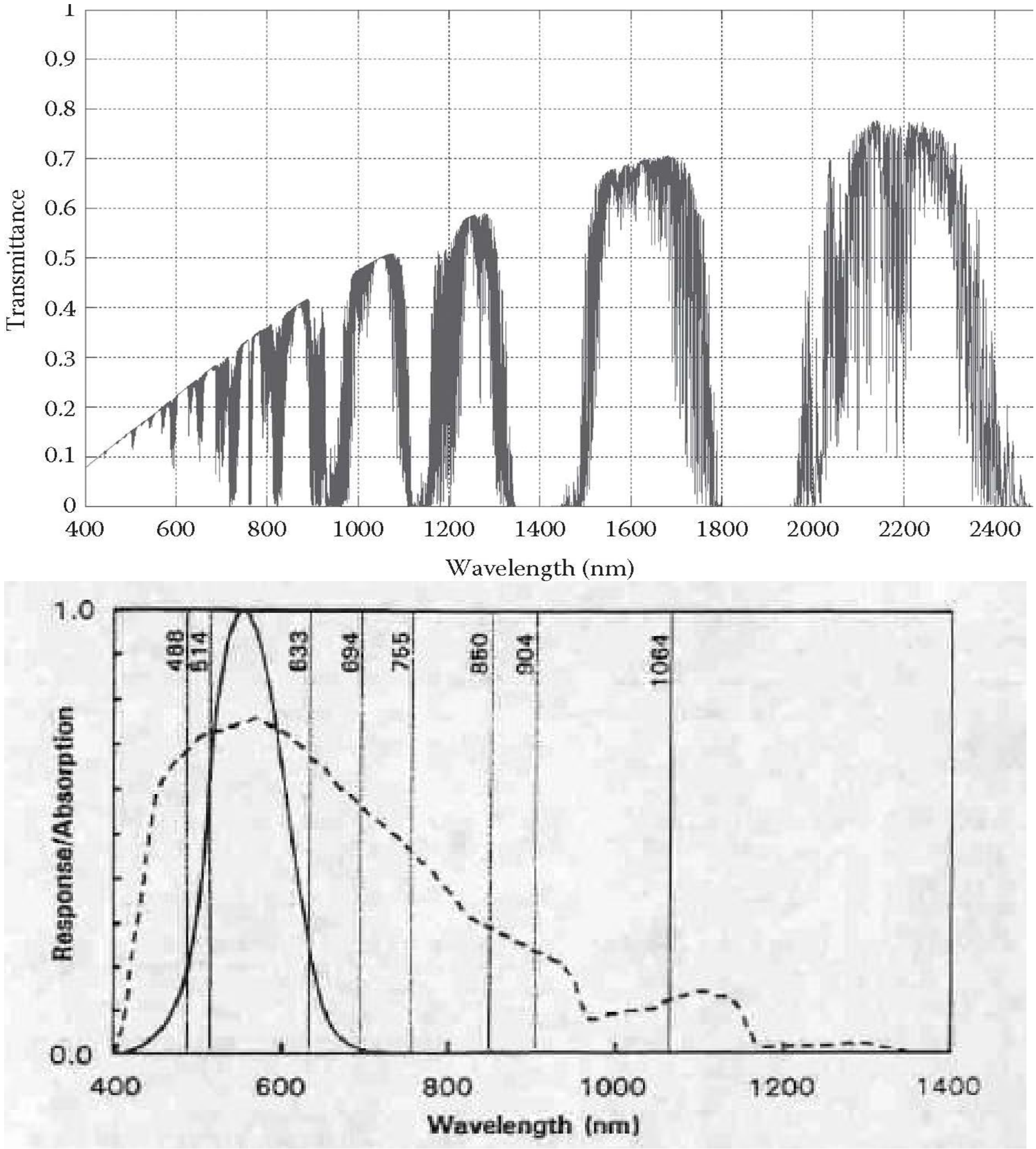

Figure 1.3: 1550nm benefits: (Top) Atmospheric transmittance windows per wavelength (Bottom) Response/Absorption of human eye per wavelength. Credits:[9, 10]

1.3.2 Probabilistic Constellation Shaping

Getting closer and closer to Shannon limit is the main goal of any telecommunication system, as the channel capacity and, consequently, the achievable bit rate is maximized. The reason for this eager search of higher throughputs has been already pointed out in the previous chapter, but there can be other reasons to enhance existent transmission systems for example improving their transmission distance or adptability to channel conditions.

In dealing with optical wired fibers, it's useful to briefly recall what Forward Error Correction (FEC) is. FEC is a practically implemented coding technique , widely used in optical networks, with the goal of lowering as much as possible the transmission error at the receiver side thanks to redundant bits that detect and correct errors. It is the obliged choice to push transmission quality towards Shannon limit and obtain good results quantifiable in BERs in the order of 10^{-15}. Anyway, FEC is not enough; in fact, as demonstrated by Shannon, to reach AWGN capacity, the source must be continous and gaussianly shaped [15].

Conventional modulation formats use uniform distributions on the constellation points leading to disadvantages such as power inefficiency of up to 1.53 dB [15] and flexibility that can be achieved only by supporting different combination of codes and modulations [16]. To this purpose, constellation shaping, that tries to mimic a continous gaussian shape over a discrete modulation, has been evaluated both in geometric shaping and probabilistic shaping with the latter showing more benefits [17]

PCS is a new technology, already developped at industry level, allowing transmissions in the order of Tbit/s [18]. Generally speaking, in traditional modulation formats every symbol has the same probability to be transmitted; for instance, in a 64 Quadrature Amplitude Modulations (QAM) transmission every symbol has 1/64 of probability to be launched. This new paradigm, instead, works on probability of occurrence of the constellation points instead of their spatial location and as result, a gaussianly shaped distribution to equidistant symbols is obtained. The criterion is the following: the lower the energy of the symbol, the higher the probability to be transmitted. A graphical representation of uniform distributed QAM and gaussianly distributed QAM can be seen in Fig. 1.4.

At practical implementation levels, the winning configuration is the Probabilistic Amplitude Shaping (PAS) that concatenate a Distribution Matcher (DM) with a FEC encoder. DMs can be of different types [16], and their goal is to do a rate adaptive shaping. They transform a sequence of uniformly distributed input bits into an output sequence of symbols from an alphabet A with a desired distribution [19]. The best DM is the Constant Composition Distribution Matcher (CCDM) whose work is to fix number of occurrences of M-ary pulse amplitude modulation (MPAM) symbols in each block [20] and is the same method applied for this study. By doing this, the FEC code can be fixed and by just arranging the distribution of the constellation, is possible to adapt and shape the modulation to the channel conditions [17]. Theoretically, the best distribution is found to be the Maxwell-Boltzmann distribution because of its ability to maximize the entropy (but in practice without the squared modulus because of implementation issues [21].)

As afore-mentioned, benefits are not just in terms of capacity since PCS, for example, allows to either transmit at higher distances (from 7 to 40% [22]). PCS can enable an adjustment of the transmission rate with very fine granularity regarding given reach and link-level requirements. Its major benefits are recapped in Fig. 1.5.

Apart from wired transmissions, PCS perfectly fits with FSO because is able to take into account high instability typical of a FSO channel by continously adapting the transmitted bit-rate to channel conditions. In this thesis,it's not only demonstrated how PCS can help in achieving very high transmission rates required for a high capacity communication but also how, thanks to the use of channel prediction, it can take into account channel variations and adapt the transmission rates supported by the SNR of the channel at that moment based on those predictions.

While PCS is a solidly tested and industrially available technology (Nokia PSE-3 chipset is present on the market), FSO implementation is still not very diffuse. Many theoretical studies have been done in order to characterize a FSO channel by proposing many statistical models based on the type of impairment experienced by it (e.g. lognormal model for weak turbulence conditions , gamma-gamma for strong

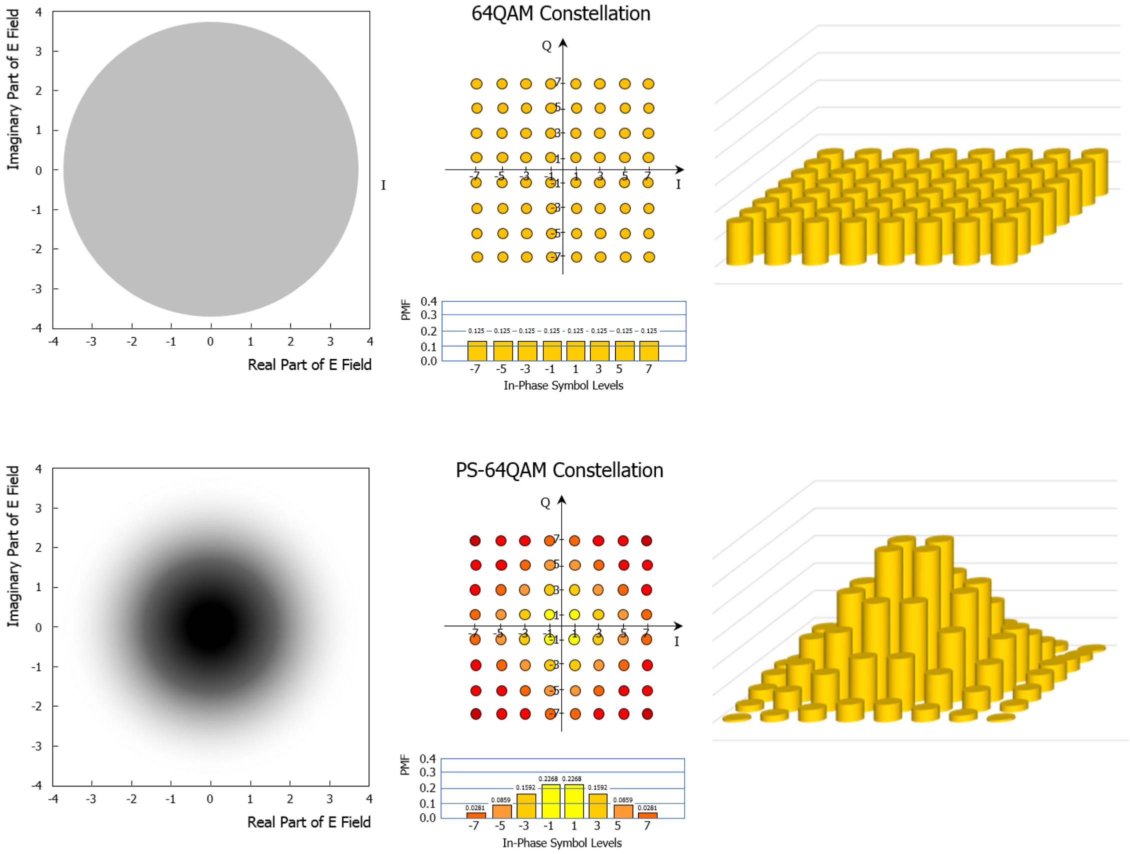

Figure 1.4: PCS 64-QAM vs Uniform 64-QAM. From : `http://opticalcloudinfra.com/index.php/2017/08/04/getting-closer-shannon-limit-constellation-shaping-34/`

turbulence, malaga as a generic one ecc.).

Some works have already been done [23] but further practical validations are needed.

The purpose of this thesis is to analyze in details these studies by mixing the two presented technologies, develop channel prediction algorithms to both counteract typical FSO impairments (by proving rain resilience) and enhance system performances, with the final goal of giving it a more practical and developable behavior.

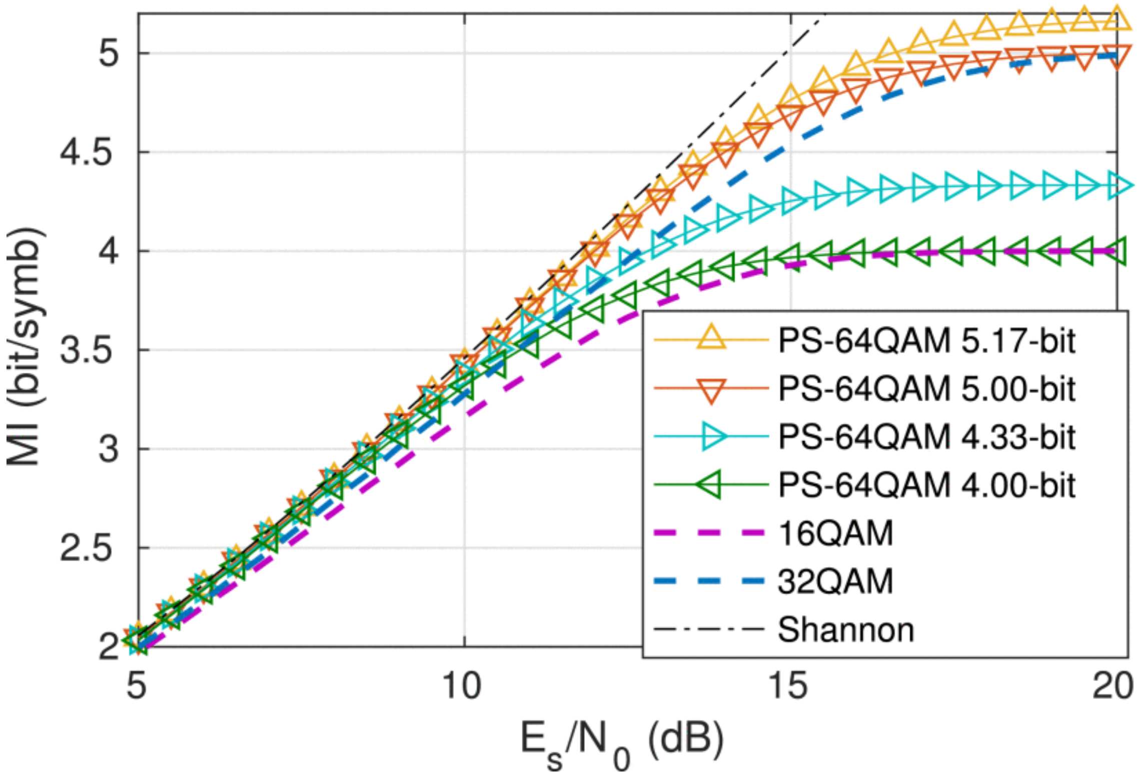

Figure 1.5: PCS advantages over traditional modulation formats in terms of mutual information in an AWGN channel. Credits: [21]

Chapter 2

FSO channel analysis

The first step of this work consists in evaluating the received optical power by using a very simple setup with the goal of characterizing the FSO link loss, that is time-varying. Transmission in the air occurs in a linear channel, i.e. non linearities and chromatic dispersion losses are not taken into account. Correlation among collected samples is then calculated and exploited in order to create low complexity algorithms to predict channel loss. After that, channel analysis is performed studying signal reception over different environmental conditions to see outdoor FSO link response.

2.1 Experimental setup

The overall experimental setup is shown in Fig. 2.1 and the involved instrumentation is the following :

- $1550\,\mathrm{nm}$ laser
  - Source laser emitting with an output power of up to +11 dBm.
- 55m free space link and mirror
  - The 55m link is the result of a 27.5m doubled thanks to the use of a mirror. Anyway, mirror's most important feature is related to the beam focusing over the receiving front end (otherwise the beam would diverge too much and the received power would be too low).
- Collimators
  - Two collimators of the same type are used. One sends the light up to the mirror while the other collects the incoming beam. They have a 24mm diameter, a 37.13mm focal length and a divergence angle of 0,017° whose numerical aperture is of 0.24.
- Power meter and pc
  - To collect power samples, readings from a portable power meter are collected thanks to a MATLAB® script that records the values with a sampling period (T_s) of 4s. This value is thought first by considering that link loss is time-varying but variations are slow, in the order of the minute, so the sampling theorem is respected, and then in order to let instrumentation safely refresh after each power acquisition.

It is worth noting that the overall system used for this experiment is mostly manual, i.e. both collimators and mirror need to be adjusted manually by working on screws they are equipped with. This may have an

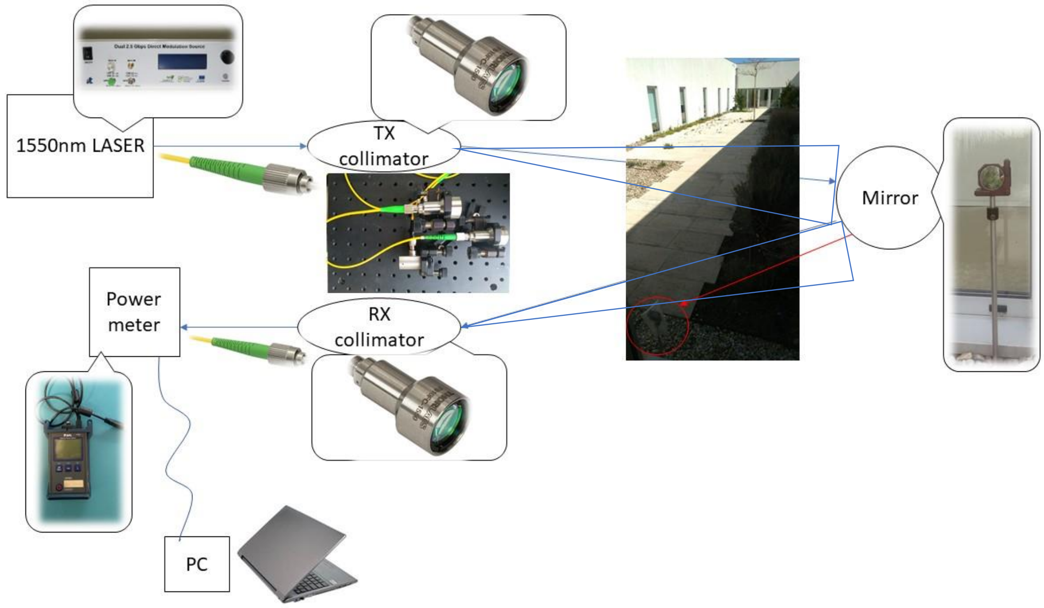

Figure 2.1: Free-space optics experimental power measurement setup

impact on the ease of reaching the optimal focusing point. Another peculiarity of the setup is that optical amplification is avoided to keep costs low, this means that the received optical power plays a very important role on the system performance, that strongly depend on the FSO time-varying attenuation, so it's important to properly characterize it.

2.2 Channel memory and prediction

The main difference between optical wired and wireless communications is the channel variability; in fact, the formers provide stable power at the receiver front end while for the latter the variations can also be very high. The signal that is going to be analyzed has been acquired during a rainy day. The impact of the weather is better discussed in the next section, here is used just to highlight how variable a FSO channel can be and what impact these variations can have.

In Fig. 2.2 two kind of variations can be highlighted, one very fast, characterized by instantaneous power jumps of even almost 3dB, and another one way smoother due to the environment changes. It can be clearly seen that the link loss is time dependent so there is the need to characterize this dynamic behavior because, in a complete transmission system, in presence of a too small signal to noise margin (whose role is better explained later), it may harm the communication up to the point of a worst case scenario in which the signal is lost.

The idea is then try to find a way to predict these variations in order to attenuate their impact on the transmission quality.

Analyzing in details the received signal, a certain trend can be noticed among collected samples (most relevant highlighted in red in Fig. 2.2) suggesting time correlation in the FSO channel and the best way to prove it is by performing an autocorrelation analysis. The result obtained confirms inter-dependency among adjacent samples as can be seen by looking at the peaks of Fig. 2.3 thus a general channel behavior can be tracked.

This opens a quite interesting scenario in which this property can be exploited in order to adapt key

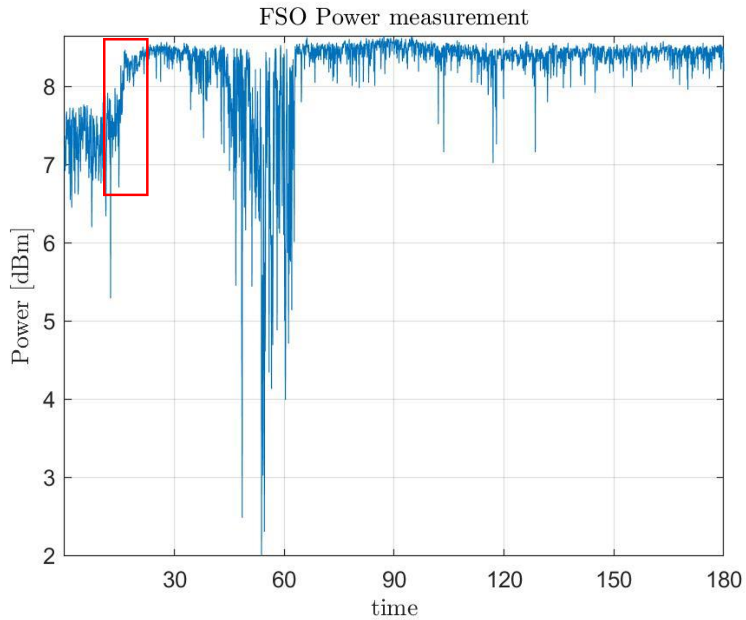

Figure 2.2: Free space optics received signal power and samples inter-dependency (highlighted in red)

transmission parameters, such as transmitted power, modulation format and data rate to avoid signal loss. Because of that, in Chapters 3 and 4 the advantages of adapting transmission rate to channel conditions will be explored.

Another way to exploit the channel memory and use it to optimize the extraction of a system model, is by building different theoretical predictors. They all rely on a Moving Average (MA) function, basically a FIR filter, but it can be shown that treating memory differently (i.e. working on the number of taps) is possible to obtain different results. The presented algorithms are: a fixed memory depth moving average (MA-fixed), an adaptive memory depth moving average (MA-adaptive), a moving average with feedback and proportional derivative terms (MA-feedback) and, in the end, the combination of the MA-adaptive and the MA-feedback (MA-adaptive-feedback). The goal of every estimator is to estimate in the best possible way the FSO channel and, to evaluate the estimation quality, the Mean Square Error (MSE) defined in Eq.[2.1] between the actual measured sample (x[n]) and the predicted one (y[n]) is calculated.

$$\mathrm{MSE} = \frac{1}{N_{samples}} \sum \left[y(n) - x(n)\right]^2 , \tag{2.1}$$

In next subsections, x[n] will refer to the same dataset from which Fig. 2.2 is derived. All the subsequent studies are performed offline i.e. the algorithms and their performance are evaluated a-posteriori over the full power vector and all the results are summed in Table 2.1

2.2.1 MA-fixed

The easiest way to implement an estimative algorithm is to apply a moving average with fixed number of taps set at the beginning. This is suboptimal in the sense that once the number of taps is decided , and this may require a calibration phase at the beginning of the measurements , it will be fixed for the rest of the transmission and it doesn't adjust to the channel reponse changes over time. Depending on the number of taps, the filtering effects can be different: if the number of taps is too large, the filter will basically behave

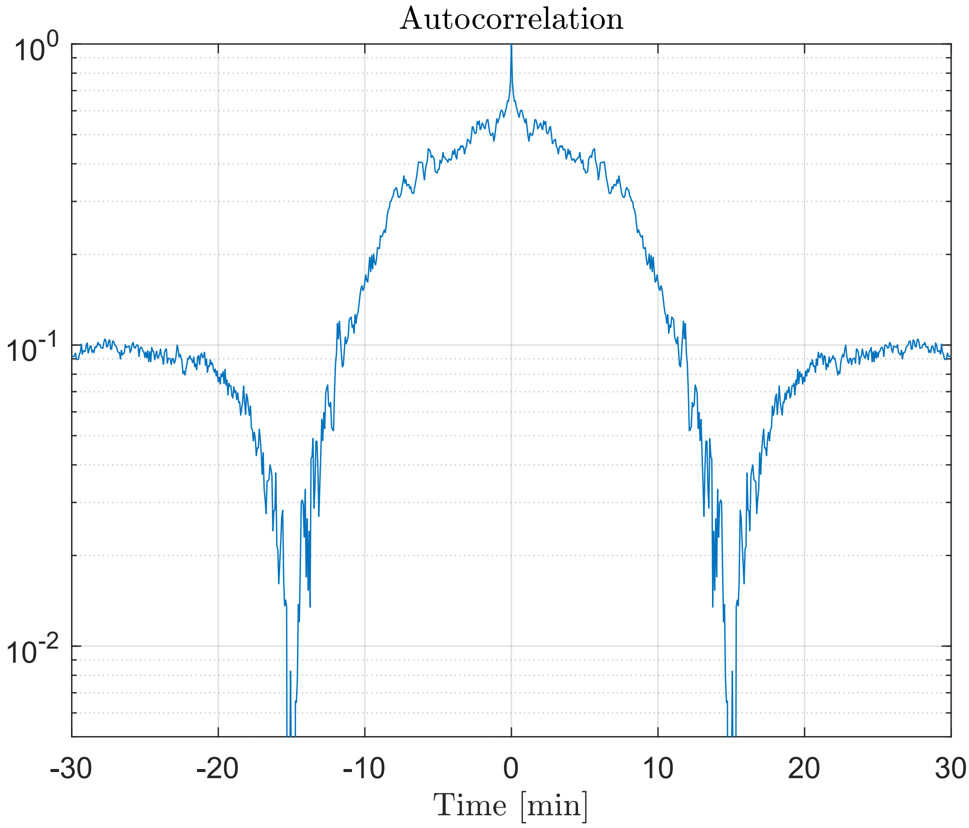

Figure 2.3: Autocorrelation of the power vector of Fig. 2.2

like a low pass filter i.e. it will filter out every high frequency variation and the higher the number of taps the stronger the effect. On the other hand, if the number of taps is too low, the algorithm will tend to follow every kind of variation and that's bad in presence of overimposed random spikes even if the mean trend is stable. The effect of different memory depth can be seen graphically in Fig. 2.4.

A mathematical description of the filter is provided by the formula 2.2.

$$y(n+1) = \frac{1}{N_{\text{taps}}} \sum_{k=0}^{N_{\text{taps}}-1} x(n-k) \tag{2.2}$$

where N_{taps} stands for number of memory samples. A block diagram is also sketched in Fig. 2.5;

The algorithm can rely on the advantage of being easy to implement, fast and not computationally expensive but the performance in terms of MSE is the worst[1].

2.2.2 MA-feedback

This algorithm, in addition to the previous MA-estimator, exploits the previous estimation error as well as the increment between the current and previous power information. In other words, now the system has a

[1]The number of taps is optimized by minimizing the MSE over the first 20 minutes of acquisition time.

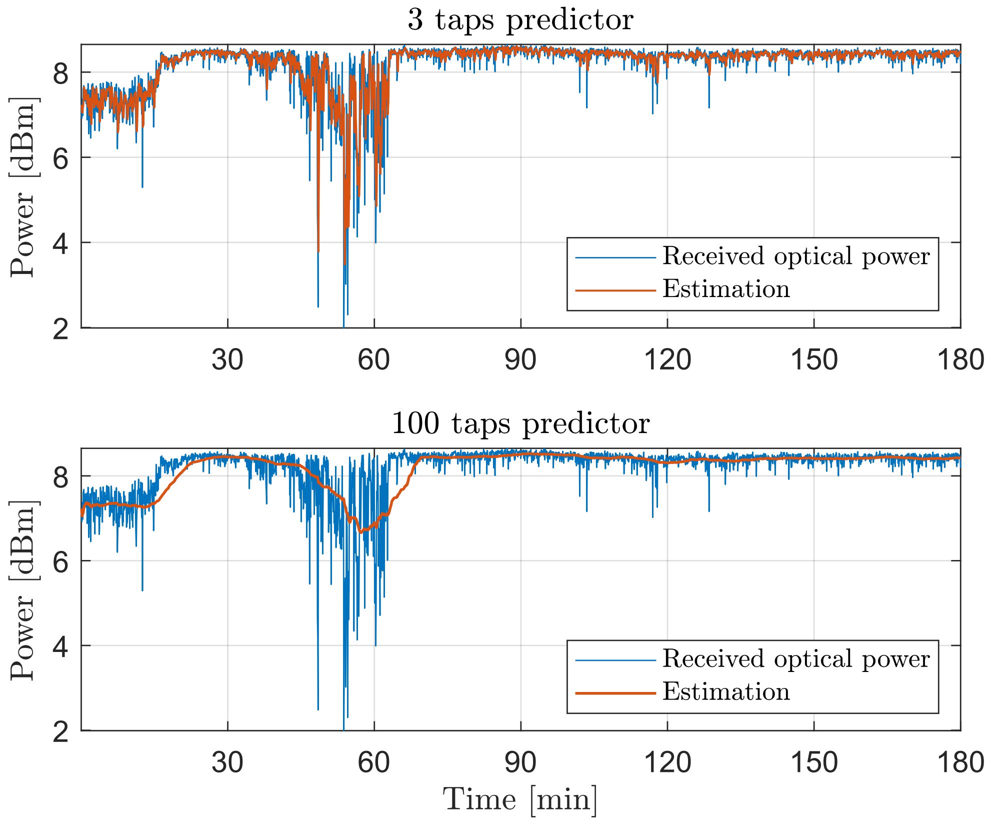

Figure 2.4: Impact of the number of taps on a moving average estimator

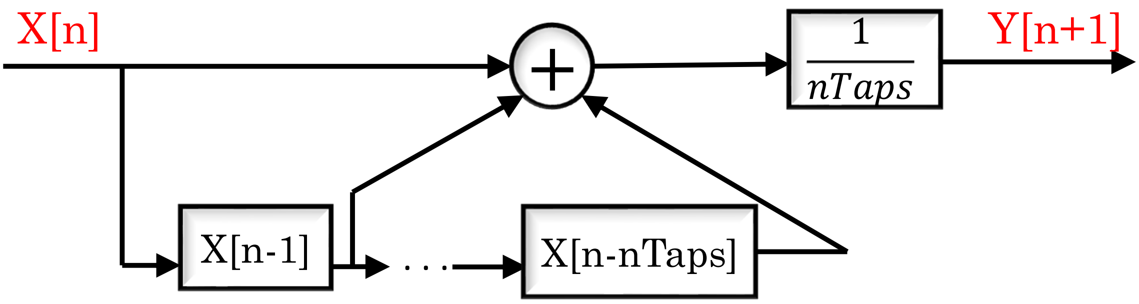

Figure 2.5: MA-fixed block diagram

differential feedback. This is done to partially neglect spikes over the signal and in the same time to check if the general behavior is changing. Whenever the error increases, the estimation error allows the program to neglect the differential term by fading its effect. In formula 2.3, ϵ and δ are the terms that are respectively encharged of following the main signal trend and filter out the spikes.

$$y(n+1) = \frac{1}{N_{\text{taps}}} \sum_{k=0}^{N_{\text{taps}}-1} x(n-k) \frac{1}{1+\delta(n)+\epsilon(n)}, \tag{2.3}$$

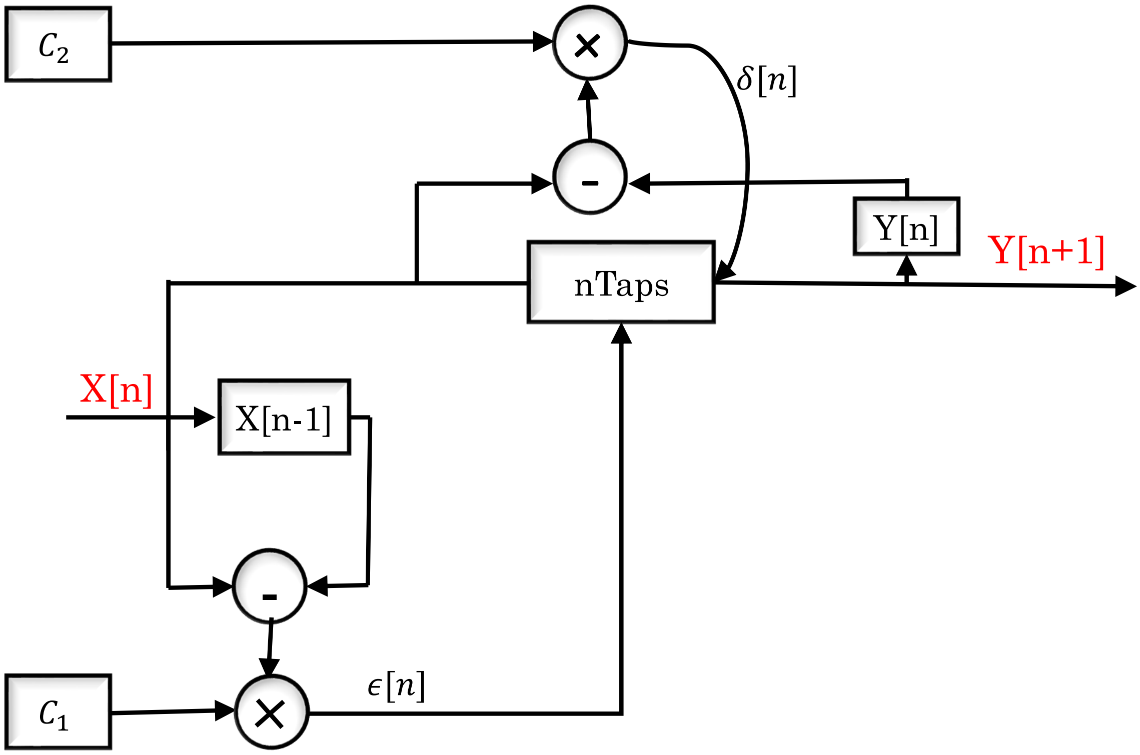

Figure 2.6: MA-feedback block diagram

$\epsilon(n)$ takes into account the previous estimation error,

$$\epsilon(n) = (y(n) - x(n-1)) \cdot C_1 \tag{2.4}$$

and $\delta(n)$ is a proportional derivative term,

$$\delta(n) = (x(n) - x(n-1)) \cdot C_2. \tag{2.5}$$

The costants are needed to weight both differential and feedback action and they are as well MSE-optimized over the first 20 minutes of acquisition time to be C_1= 0.001 and C_2= 0.020. The number of taps is the same used for the MA-fixed case. A block diagram is depicted in Fig. 2.6 where the nTaps box refers to the same scheme of the MA-fixed.

The algorithm is faster, in terms of processing time, than MA-adaptive algorithm but has the delicate problem of dealing with feedback and constants C_1 and C_2 ; in fact, first of all, if constants are badly set, the algorithm can diverge and second, to properly set their values, another periodic calibration phase is needed. In MSE terms the result is better than the MA-fixed but worse than the MA-adaptive.

2.2.3 MA-adaptive

As stated before , the problem of the previous estimators is the lack of real time channel variations adaptation i.e. as soon as there is an acquisition, they predict the next sample with always the same number of taps thus not taking into account recent history. This algorithm, instead, has the very nice feature of adapting to channel variations by always finding the best number of taps so that the tracking capability is optimized. To give the algorithm a bound, at most 100 past samples are taken into account. With a sampling period of 4 seconds, 100 values are able to consider channel variations of more than 5 minutes that is a reasonable time to account for both fast and slow variations.

The working principle is the following : any time a new sample is acquired, the algorithm uses the past 100 previous samples to find the optimum number of taps minimizing the MSE between the 100 previous predicted samples and the 100 previous measured samples. Once the optimum number of taps is found, this is used by the filter to predict the next power value and the operation is performed on a per-sample basis. This behavior can be summed by forumla 2.6 and a block diagram of the predictor is presented in Fig. 2.7.

$$y(n+1) = \frac{1}{N_{\text{taps}}(n)} \sum_{k=0}^{N_{\text{taps}}(n)-1} x(n-k). \tag{2.6}$$

MA-adaptive provides good performance in MSE terms but the dynamic adaptation of number of taps in the moving average comes at the cost of being computationally intense.

2.2.4 MA-adaptive feedback

The last presented estimator is built by mixing the the MA-adaptive algorithm with the MA-feedback one. The working principle is to follow the same strategy used for the MA-adaptive to extract the best number of taps and use them to feed the MA-feedback estimator. It is able to produce the best MSE results but it's also the most costly and, as for the MA-feedback, the problem of proper coefficients set is still present. In formula 2.7 the coefficients have the same values as in 2.4 and 2.5. A block diagram is also provided in Fig. 2.8 and the nTaps box has the same meaning as for the MA-feedback scheme.

$$y(n+1) = \frac{1}{N_{\text{taps}}(n)} \sum_{k=0}^{N_{\text{taps}}(n)-1} x(n-k) \frac{1}{1+\delta(n)+\epsilon(n)}, \tag{2.7}$$

Table 2.1: Performance comparison of the presented estimation algorithms

	MA-fixed	**MA-adaptive**	**MA-feedback**	**MA-adaptive-feedback**
MSE	0.1747	0.1109	0.1485	0.0989
Cost (processing time [s])	0.02	112.93	0.11	113.52
Max Squared Error	26.63	20.86	22.66	18.94

The prediction results of the estimators are presented numerically in a compact way in Table 2.1 and graphically in Fig. 2.9.

What can be said is that if cost is not an issue, the most obvious choice is the best performance algorithm otherwise even the simplest one can be used as the difference among them is not that high. The maximum squared error is also displayed as it captures the impact of error spikes, which might be important to consider in case of interest in having a reliable system.

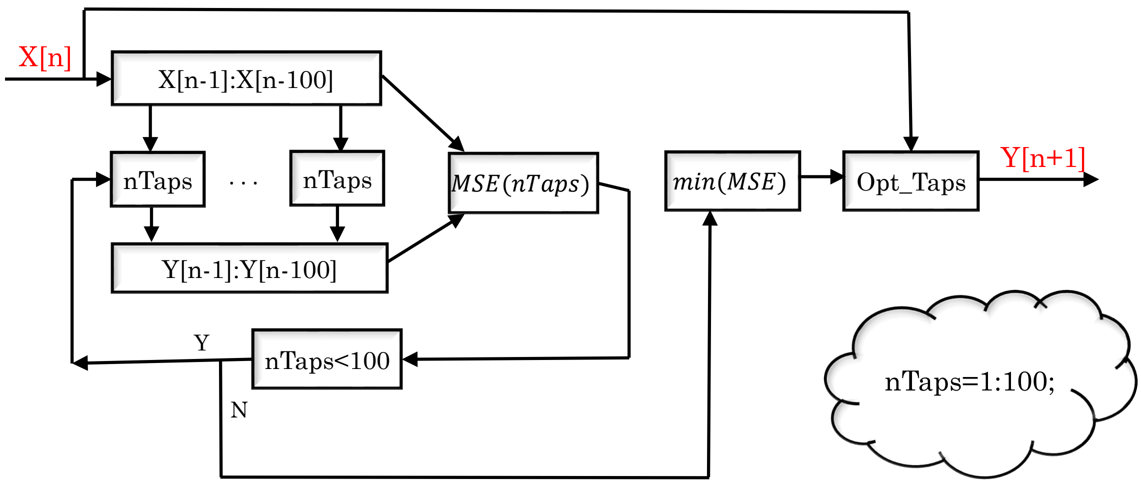

Figure 2.7: MA-adaptive block diagram

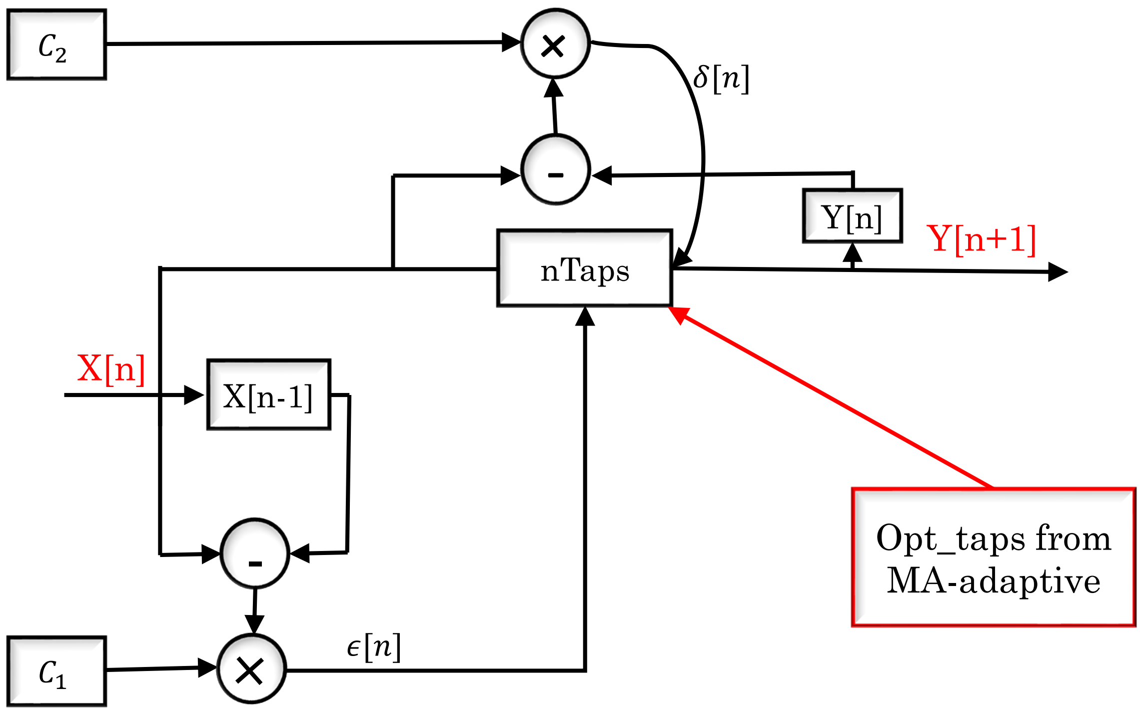

Figure 2.8: MA-adaptive-feedback block diagram

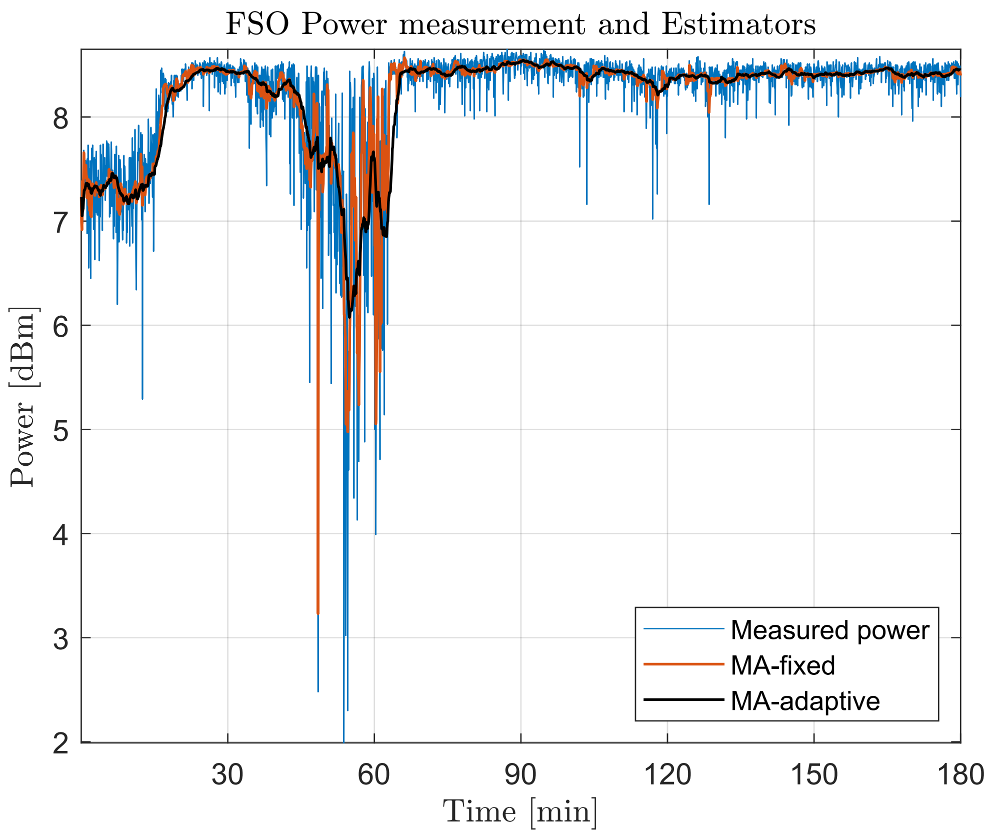

Figure 2.9: Measured received and estimated power with best and worst MSE-performance predictors to show their similar performance

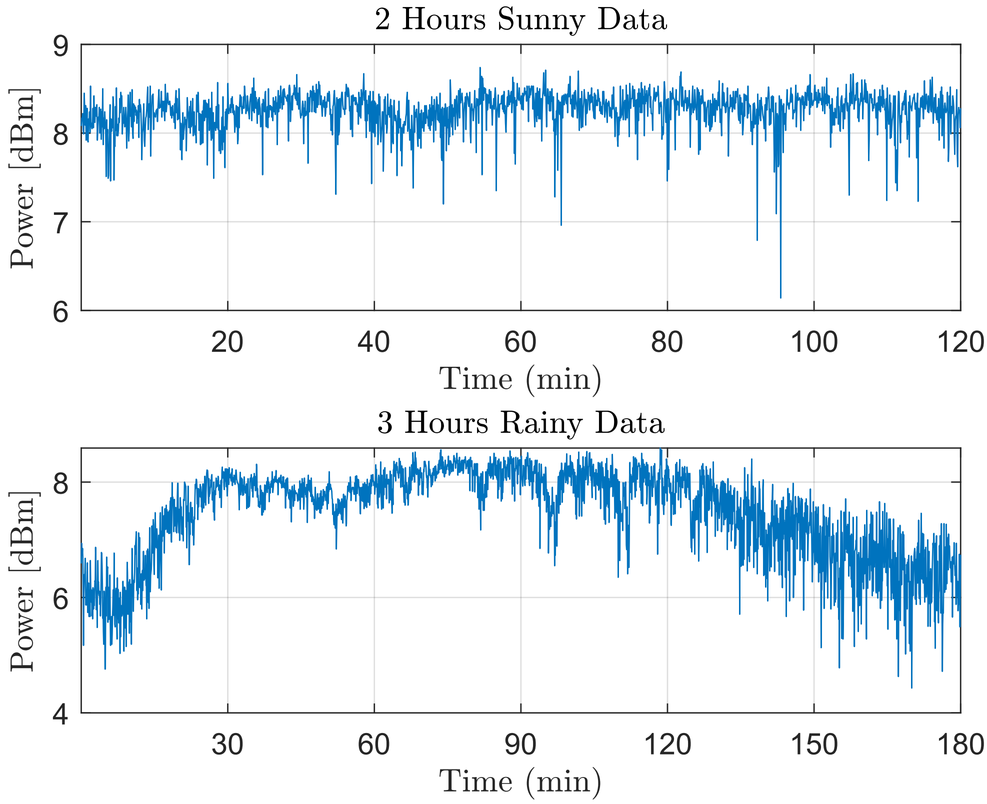

Figure 2.10: Received optical power for different FSO channel conditions

2.3 Weather impact

The main impairment for an outdoor FSO setup is the weather and its related atmospheric turbulence. In the following, a demonstration of working system in different weather conditions is presented with the final purpose of defining different channel profiles.

2.3.1 Data analysis

By collecting power measurments with the same setup of the previous section in different days, interesting results arise by comparing what is obtained in sunny and rainy days. As can be noticed in Fig. 2.10 (top), knowing that an optical power of +11 dBm is transmitted, a 3dB attenuation is introduced in good weather conditions, considering cable,connectors and free space link losses, and no more than 7dB during rainy days (Fig. 2.10, bottom), even if in those cases attenuation may be also due to other impairments such as, for example, rain droplets falling over the mirror or the collimators.

Autocorrelation analysis, in this case, shows a very nice effect; in fact, it can clearly be noticed in Fig. 2.11 that in presence of rain, time correlation is longer . These are the effect of slow changes in weather, like for example rain rate and humidity, contributing to longer-term memory effects. Over this purpose , different weather profiles can be tracked and studied.

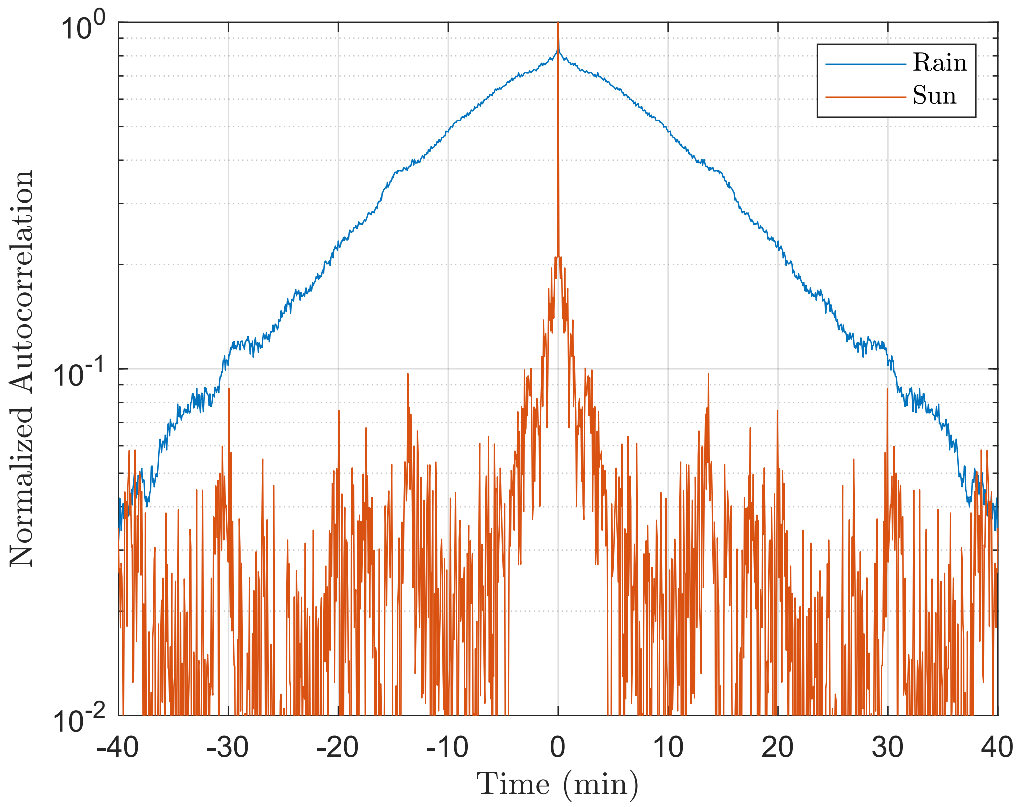

Figure 2.11: Normalized autocorrelation function of power measurements of Fig. 2.10

2.3.2 Different estimators results

Different predictors results are presented in Tables 2.2 and 2.3 and in Figs. 2.14 and 2.15.

Displaying the time evolution of the instantaneous squared-error using the MA-fixed algorithm (Fig. 2.13) is noticeable that sunny days are characterized by an overall stabilized power with isolated spikes overimposed, suggesting that they can be related with random phenomena. The MA-adaptive filter's number of taps variation, shown in Fig. 2.12, is also a good probe to justify different channel responses based on the weather : the number of taps is higher (in mean) for sunny data and lower (in mean) for rainy ones. By recalling what stated in 2.2.1, the higher the number of taps, the more the filter will behave like a Low Pass Filter (LPF) thus its main goal is to filter the noise out (the spikes in this case). For rainy data, instead, whenever the mean value changes, the filter needs to track it and that is done by lowering the number of taps making the convergence faster. Indeed, MSE is lower in sunny days while it increases quite a lot during adverse weather, because of both high and low frequency variations in those cases.

As expected, the MA-adaptive-feedback algorithm provides the best result in terms of MSE with even a higher gap with respect to the others in the rainy scenario.

The number of taps for the non-adaptive algorithms is again optimized by taking into account the first 10 minutes of acquisition and used for the overall transmission. For the constants C_1 and C_2 used in the two feedback algorithms, the optimized values are : $C_1 = 0.001$ and $C_2 = 0.0077$ for the sunny scenario and $C_1 = 0.0001$ and $C_2 = 0.026$ for the rainy one. It can be clearly seen that by taking the mean of the number of taps of the MA-adpative algorithm, the optimum number of taps is different suggesting that for a precise prediction an adaptive algorithm is preferred. It can be furtherly pointed out that even in different weather conditions, all the techniques are able to provide good approximation of the data. At the end of the rainy measurement there was an increased error related to alignment problems probably induced by the weather itself (bottom row of Fig. 2.13).

Table 2.2: Estimators response in perfect weather conditions

Estimator	MA-fixed	MA-adaptive	MA-feedback	MA-adaptive-feedback
MSE	0.04274	0.0405	0.0425	0.0368
Taps	13	27 (avg.)	13	27 (avg.)
Max Squared Error	3.36	3.357	3.554	3.5711

Table 2.3: Estimators response in bad weather conditions

Estimator	MA-fixed	MA-adaptive	MA-feedback	MA-adaptive-feedback
MSE	0.1321	0.1228	0.1297	0.0968
Taps	13	17 (avg.)	13	17 (avg.)
Max Squared Error	3.273	4.178	3.508	3.6978

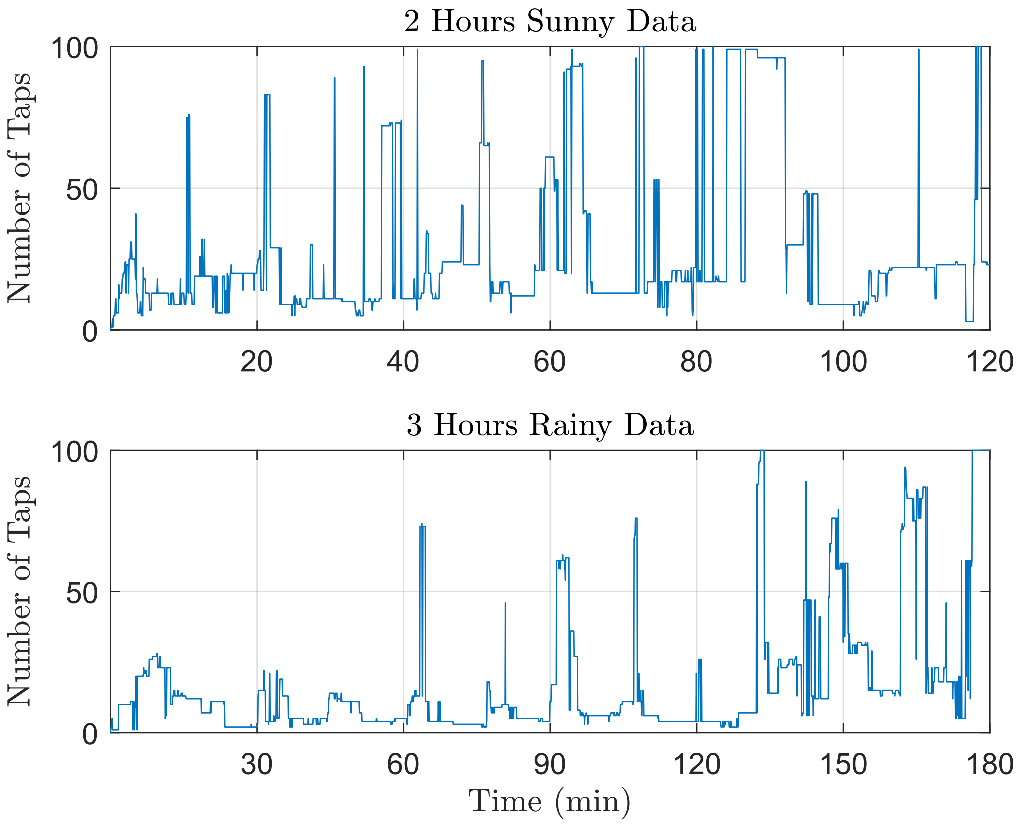

Figure 2.12: Real time variation of number of taps using the MA-adaptive algorithm for different weather profiles

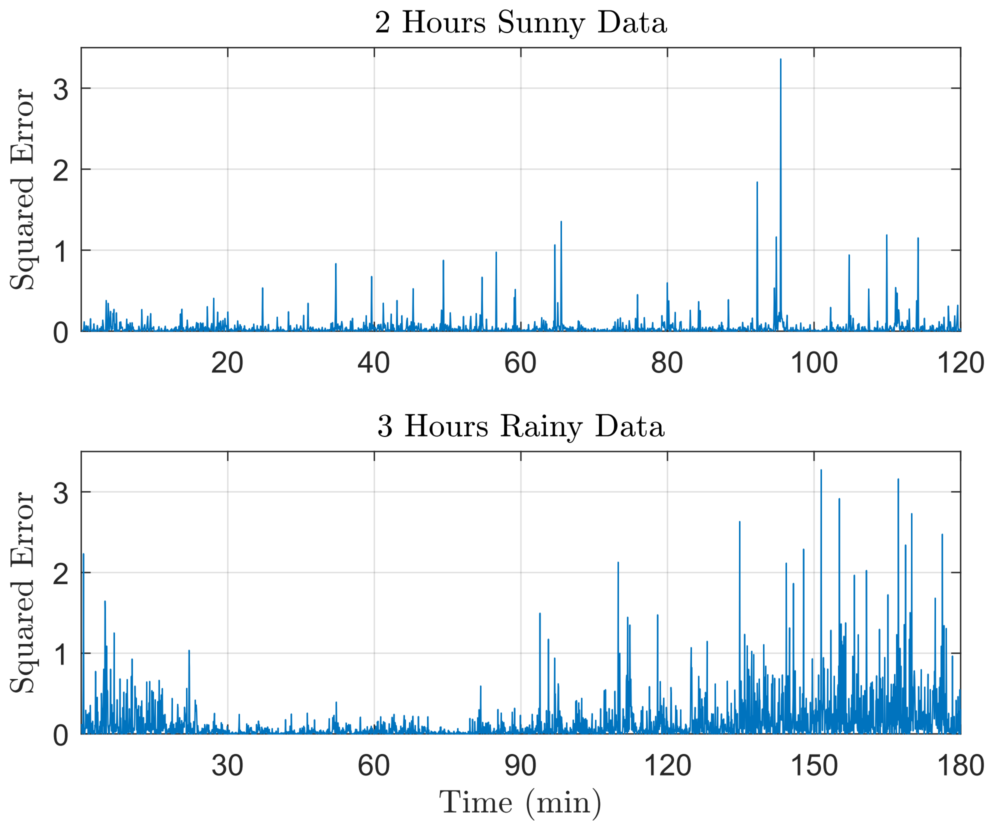

Figure 2.13: MA-fixed instantaneous squared error over time

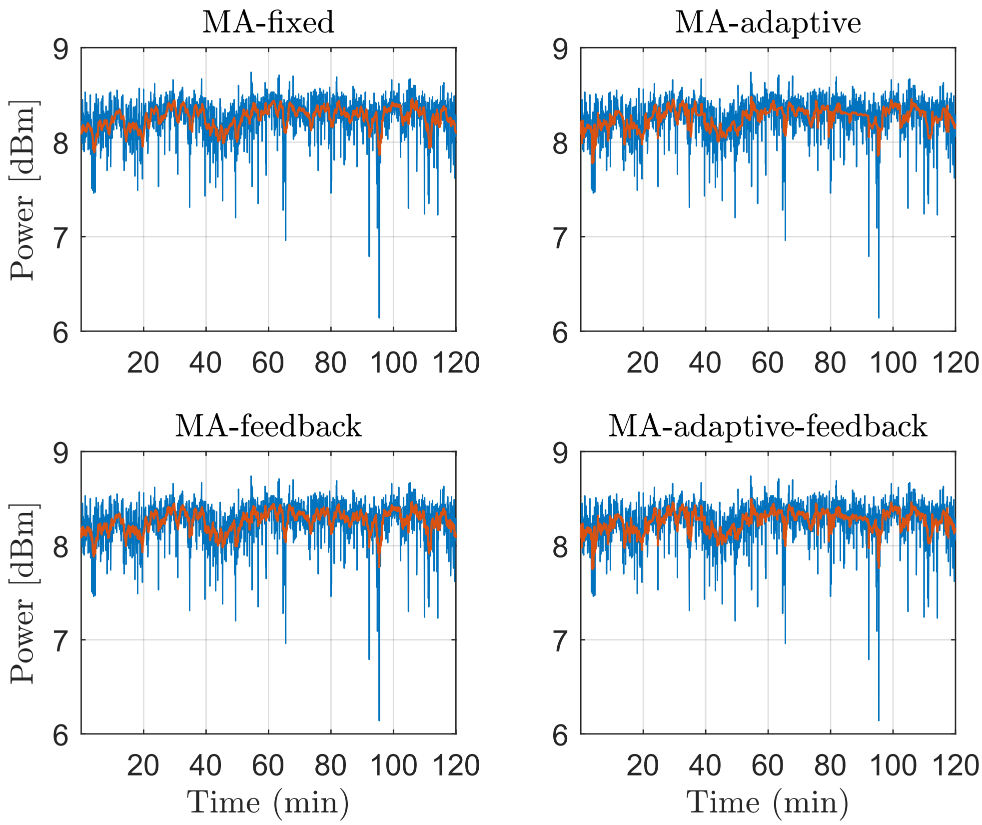

Figure 2.14: Collected power (blue) and its estimation (red) for every type of estimator in sunny scenario

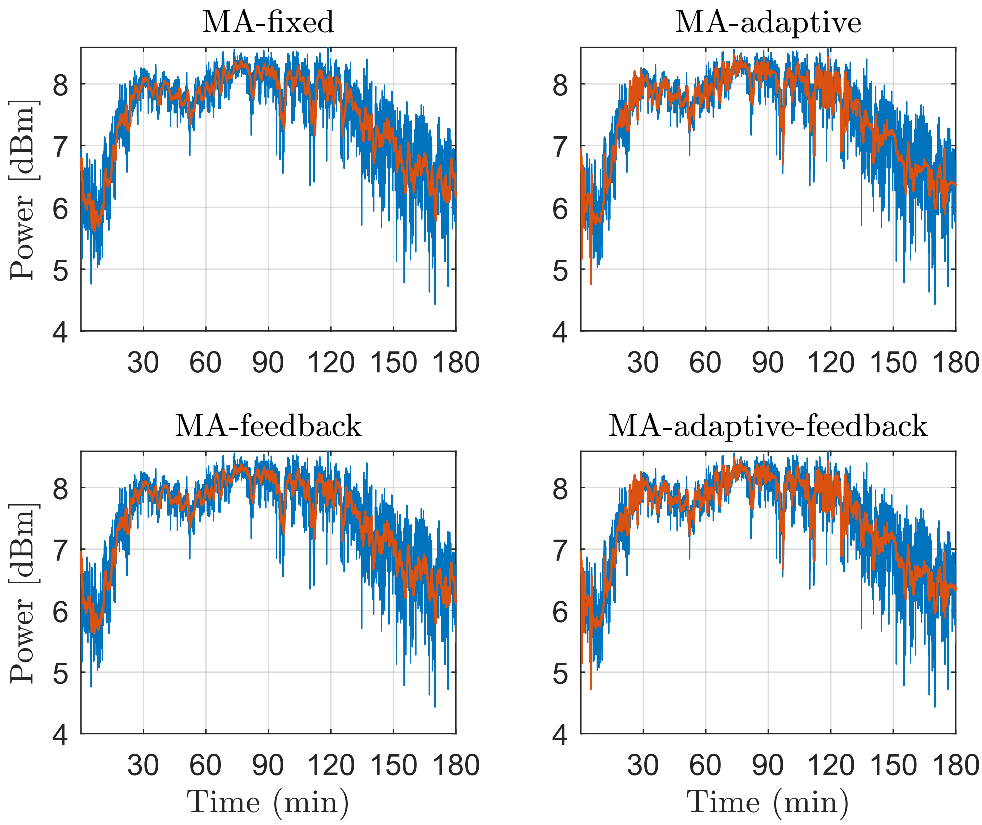

Figure 2.15: Collected power (blue) and its estimation (red) for every type of estimator in rainy scenario

Chapter 3

Offline processing

In telecommunications, to evaluate the quality of a received signal , the most important parameter to consider is the SNR, i.e. how larger is the signal with respect to the noise floor. It has many implications on the transmission performances as Shannon's formula relates it with channel capacity.

In the following, SNR values are first guessed from the power vectors of the previous chapter and then used to emulate a real FSO transmission.

3.1 Simulation scheme

In this offline investigation a linear offset to the curves of Fig. 2.10 is applied to translate power values into SNR values. The offset is calculated considering the difference between the maximum measured power and a maximum SNR of 15 dB , which is a typical received SNR value using a complete transmission scheme as in [23] when minimum attenuation from the FSO channel is considered. The curves under investigation in the following sections are represented in Fig. 3.1.

Offline processing means that the full measured vector is already available as well as the predicted one (as in the previous chapter) so any kind of calculation is done over the full vector and not step by step in real time.

This simulation scheme relies on some important concepts such as Normalized Generalized Mutual Information (NGMI),Entropy (H), Achievable Information Rate (AIR) and others that need to be quickly introduced as they are going to be the reference metrics to analyze the system performance as well as the same parameters used in the next chapter.

The NGMI represents the number of information bits that can be reliably decoded from each transmitted bit and, as showed in [24], it can be used to predict post- FEC BER. FEC overhead ($\mathrm{FEC_{oh}}$) is often set to 20% and in order to guarantee an error-free transmission the NGMI at the receiver should be at least greater than some specific values based on the type of FEC decoder used. Theoretically speaking, when using a 20 % $\mathrm{FEC_{oh}}$, NGMI must be at least equal to $0.8\overline{3}$ but for practical implementations this number must be higher. Here, a value equal to 0.9 is taken into account as a possible conservative value but is not associated with any specific FEC. In the end, it will be a clear indicator about the sustainability of the channel with respect to the transmitter requirements because if the NGMI is below its FEC-imposed threshold, then an error-free communication cannot be guaranteed.

The entropy H is the direct link to evaluate the throughput performance of the system as it can be related to the AIR through the formula $\mathrm{AIR} = H - H_{\mathrm{FEC}}$ where $H_{\mathrm{FEC}} = (1 - R_{\mathrm{FEC}}) \cdot log_2(M)$. M is the constellation size and $\mathrm{R_{FEC}}$ is the FEC rate that represents a data to correction bits ratio and is equal to $\frac{1}{(1+\mathrm{FEC_{OH}})}$. The AIR represents the number of information bits per symbol that can be reliably transmitted through a channel and its usage as performance metric in optical communications is growing lately [25]. In

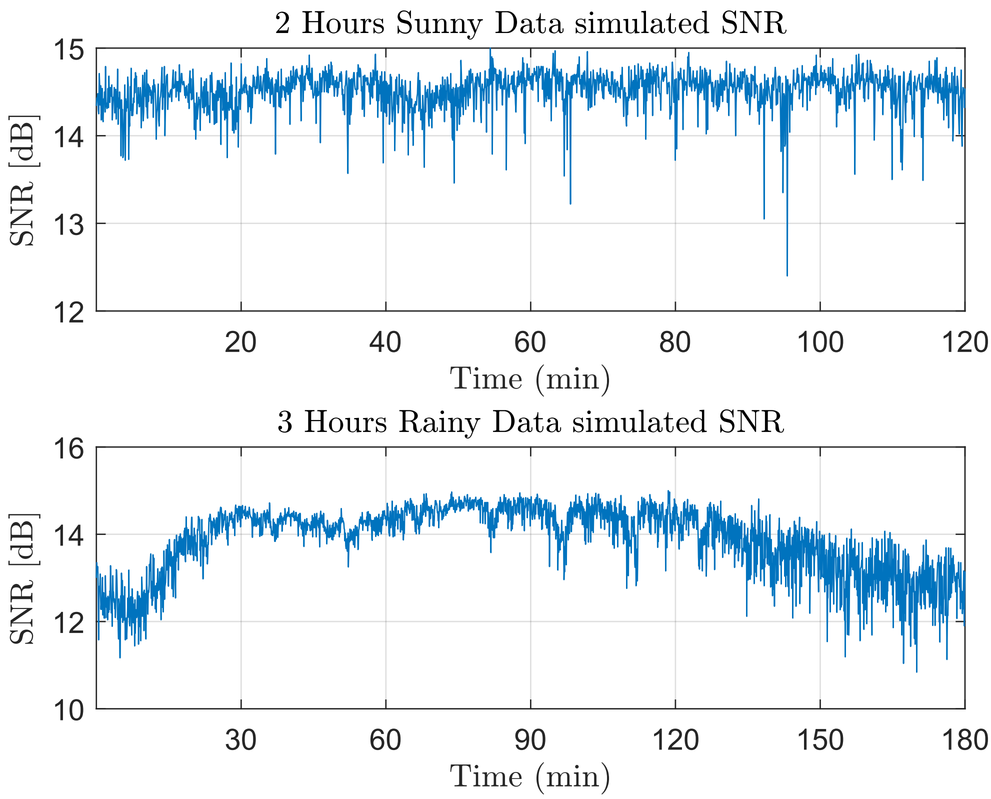

Figure 3.1: SNR curves obtained from power measurements of Fig 2.10

order to extract the bit rate from the AIR, the used formula is the following :

$$R_b = \mathrm{AIR} \cdot N_{\mathrm{pol}} \cdot R_s \cdot R_{\mathrm{pil}} \tag{3.1}$$

where $\mathrm{R}_{\mathrm{pil}}$, is the pilot rate i.e. how many of the transmitted symbols are used to probe the channel, R_{s} is the symbol rate expressed in baud ($\frac{symbols}{s}$) and $\mathrm{N}_{\mathrm{Pol}}$ refers to the number of polarizations used.

In dealing with predictors, the SNR_{margin} is an important parameter to take into account as it is used to accomodate unknown channel variations. Its role is the following : the higher it is, the lower will be the channel exploitation but the reliability will be higher as the higher the margin, the lower the probability to lose the signal i.e. the lower the probability to fall under the NGMI threshold meaning that is being asked less of what the channel can actually sustain. On the other end, by forcing a little bit the margin, it is possible to gain in capacity as the received SNR will be higher but also the possibility to lose the signal will be higher as the NGMI threshold may be crossed and an overestimation of the channel will occur.

The main actors for all the following results are some already implemented Look-Up Table (LUT)s that, given some input parameters as in formulas 3.2 and 3.3 , are able to provide H and NGMI sample by sample.

$$\mathrm{H} = f(\mathrm{SNR}_{\mathrm{predicted}}, \mathrm{NGMI}_{\mathrm{th}}, M); \tag{3.2}$$

$$\mathrm{NGMI} = f(\mathrm{SNR}_{\mathrm{measured}}, M, H); \tag{3.3}$$

where NGMI_{th} is the NGMI threshold , $\text{SNR}_{\text{measured}}$ is the actual measured SNR from the channel and $\text{SNR}_{\text{predicted}}$ is the outcome of the used estimator with the $\text{SNR}_{\text{margin}}$ already applied.

They are based on PCS, whose theoretical advantages are discussed in 1.3.2 and the practical ones are now presented.

The use of PCS allows to adapt the transmission to channel conditions which are tracked by the predictors. By simply modifying symbols' probability of occurrence it is able to automatically adapt transmission rates to the best channel conditions. Furthermore, it is able to provide some SNR margin gain (~1 dB) with respect to the other adaptive techniques.

It can be seen that the function extracting the entropy requires the predicted SNR and the constellation size as it finds the maximum possible entropy such that the NGMI_{th} is satisfied, already taking into account the SNR margin. In order to evaluate the channel sustainability, the NGMI function checks if the entropy just calculated can be sustained by the actual SNR to check how erroneous is the prediction. Again, for a bigger margin the resulting entropy will be sustainable so even if the variations in the channel are high, the error will be taken into account by the margin and the resulting NGMI value will be greater than 0.9. On the other end, for lower SNR margin , the resulting entropy will be higher and if the error among the SNR curves is high with $\text{SNR}_{\text{predicted}} > \text{SNR}_{\text{measured}}$, the transmission is not sustained by the channel and the resulting NGMI value will be lower than 0.9.

To picture this behavior,the value of $\text{SNR}_{\text{predicted}}$ can be fixed and its corresponding H value is used with the NGMI function where a vector of measured SNR from 0 to 15 is provided. The result of the usage of $\text{SNR}_{\text{predicted}} = 12$, $\text{NGMI}_{\text{th}} = 0.9$, $M = 64$ is displayed in Fig. 3.2. As expected, when $\text{SNR}_{\text{measured}} = 12$, $\text{NGMI} = 0.9$. When the measured is higher, the NGMI is greater than 0.9 because the prediction underestimates the channel while on the other end when the measured is lower, the NGMI is lower than 0.9 as a result of an over estimation.

Thanks to the use of PCS , it was possible to first of all evaluate the gain of using a predictors-adaptive transmission system over a non adaptive one. After that, the impact of the sampling frequency on the achievable rate and of the $\text{SNR}_{\text{margin}}$ on the reliability is discussed.

For all the following results, these are the simulated transmission settings :

- $\text{R}_{\text{pil}} = 15/16$
- $\text{R}_{\text{FEC}} = 5/6$
- $\text{NGMI}_{\text{th}} = 0.9$
- $\text{M} = 64$
- $\text{R}_{\text{s}} = 64$ Gbaud
- $\text{N}_{\text{Pol}} = 2$

The usage of these parameters is dictated by the laboratorial instrumentation capabilities (that will be used in chapter 4) that allow a transmission of 64 GBaud of gross symbol rate. This will guarantee, according to 3.1, a transmission of at most 600 Gbps when the PCS-64 QAM constellation is loaded with its maximum entropy of 6 bits/symbol (corresponding to uniform 64 QAM signalling).

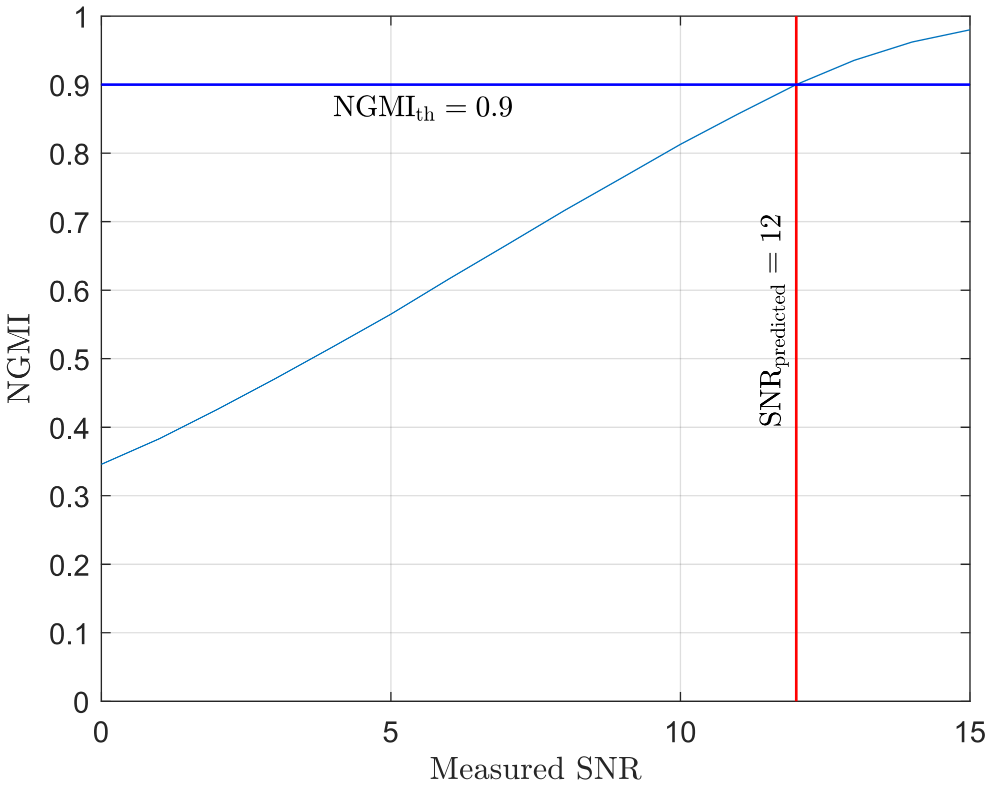

Figure 3.2: NGMI vs $\mathrm{SNR_{measured}}$ for $\mathrm{SNR_{predicted}} = 12$

3.2 Predictors gain

The usage of a non-adaptive transmission scheme is risky in a FSO environment as the channel variations may be so high that communication is disrupted. As for the number of taps for the MA-fixed algorithm, even in this case an initial calibration phase in which channel condition is studied can lead to transmission parameters settings that some time later may results erroneous.

Whenever there is underestimation, the channel is not fully exploited and on the other hand in presence of overestimation, the reliability will fall as it may happen that the signal is frequently lost. In this case, the evaluation is performed over the dataset of Fig. 3.1 in which for the non-adaptive simulation the mean value of the SNR vectors is considered. This choice is made in order to mitigate the effects of a too coarse initial overestimation or underestimation of the channel ; in this way, a reasonable fixed entropy value is provided for the whole transmission.

3.2.1 Expected results

What is expected is the following : for the non adaptive transmission, whenever the actual SNR is above the mean, there will be a reliable transmission because of the underestimation, thus the NGMI will always be above the threshold. On the contrary, when the actual SNR value is under the mean, the signal will be lost and the NGMI will be lower than 0.9 .

On the long run, the estimators will provide a large improvement because in presence of underestimation they will be able to track the SNR more precisely, thus enabling to adjust the transmitted entropy to better exploit the temporarily improved channel capacity, and when there is over estimation, they will lose the signal way less as able to reduce the transmitted entropy to adapt to the temporarily degraded channel capacity.

3.2.2 Results

To highlight the advantages of the prediction system, the most important result to look at is the accumulated capacity. Accumulated capacity refers to the cumulative sum of all the achievable bit rates during the transmission, i.e. everytime the link is properly operating (NGMI>0.9). Bit rates are calculated as in 3.1 and set to 0 whenever the NGMI is lower than 0.9. $\mathrm{SNR}_{\mathrm{margin}}$ is set to be the one giving the best average bit rate as shown in Fig. 3.3.

The difference in performance, by using different predictors, can be tracked by evaluating the accumulated capacity over time and is showed in Figs. 3.4. All the settings for the predictors are the same used in 2.3.

As expected, the best result is provided by the MA-adaptive-feedback algorithm but it can clearly be seen that the difference among predictors is not that high, at least in the short run and especially in stable weather conditions. This behavior is the same for every kind of study that is going to be presented and for this reason, for all the following results, whenever there will be a comparison between a non adaptive transmission scheme and an adaptive one, adaptive results refer to the MA-adaptive-feedback ones.

Graphical results in terms of accumulated capacity gain of an adaptive algorithm with respect to a non adaptive one are shown in Fig. 3.5.

What was expected is confirmed and when the gain is negative it means that the predicted value is erroneous so NGMI<0.9 and $\mathrm{R_b}=0$ while the mean is underestimating so NGMI>0.9 and $\mathrm{R_b}>0$. What drags attention is the difference in gain between rainy and sunny days; in fact, despite the fact that rainy measurement is one hour longer, the gain is in any case one order of magnitude greater than in sunny case. Anyway, this is reasonable because, as already stated in 2.3, variations in the mean value are higher in rainy days with respect to the sunny ones which instead are characterized by only random fluctuations around the mean. Whenever oscillations are higher, the gain in using a channel estimator is also higher and not only: for a better estimator, slightly better results can be achieved, either in terms of $\mathrm{SNR}_{\mathrm{margin}}$ or in terms of achivable bit rate for the same margin as can be clearly seen in Fig. 3.3.

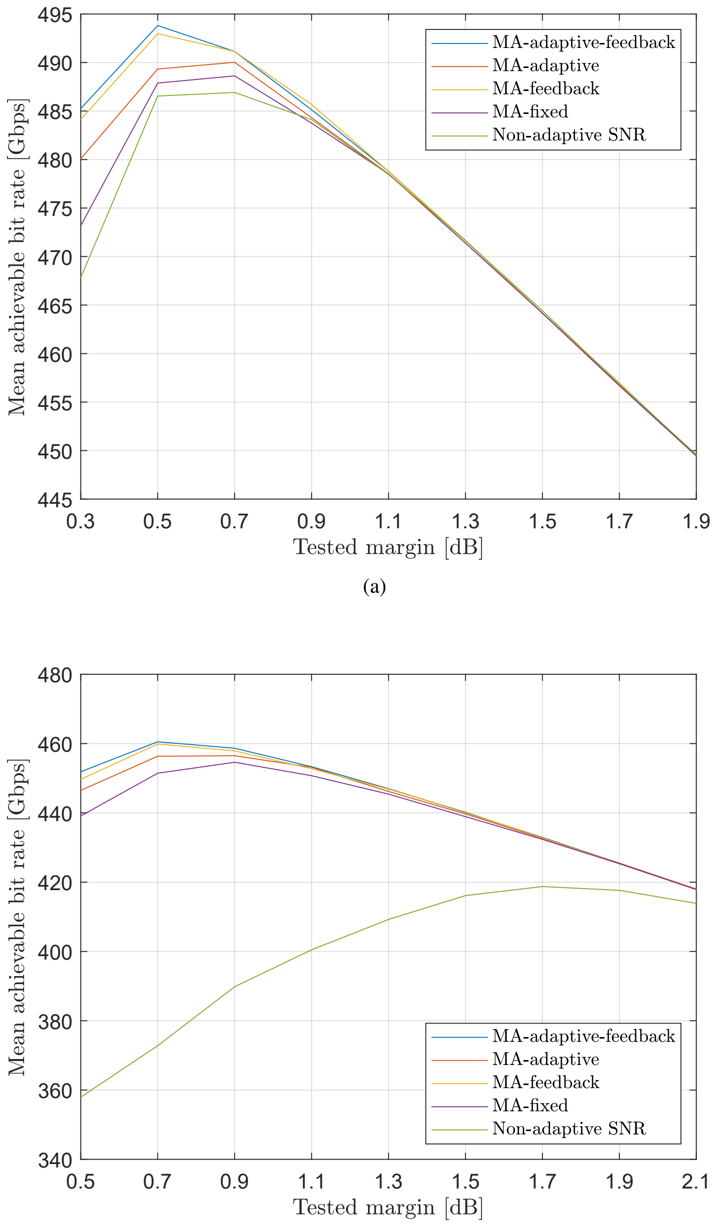

(a)

(b)

Figure 3.3: Mean achievable bit rates for different tested margins from (a) 0.3 dB to 1.9 dB with 0.2 dB granularity for sunny weather and from (b) 0.5 to 2.1 with 0.2 dB granularity for rainy weather

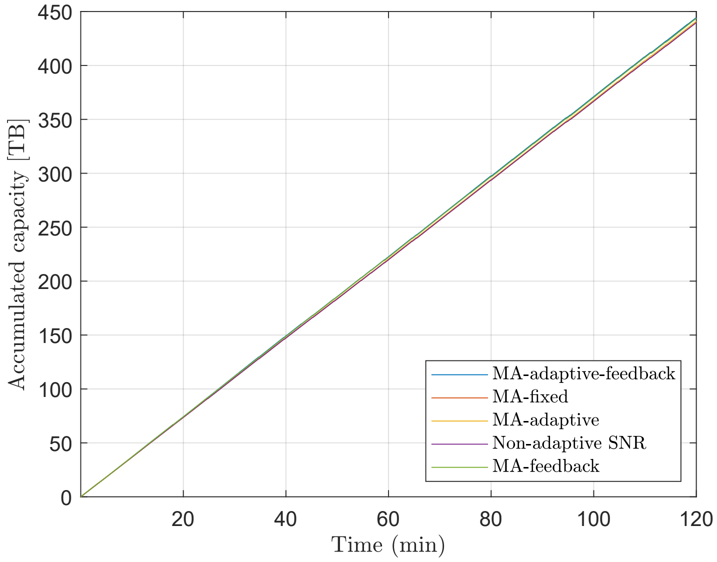

(a)

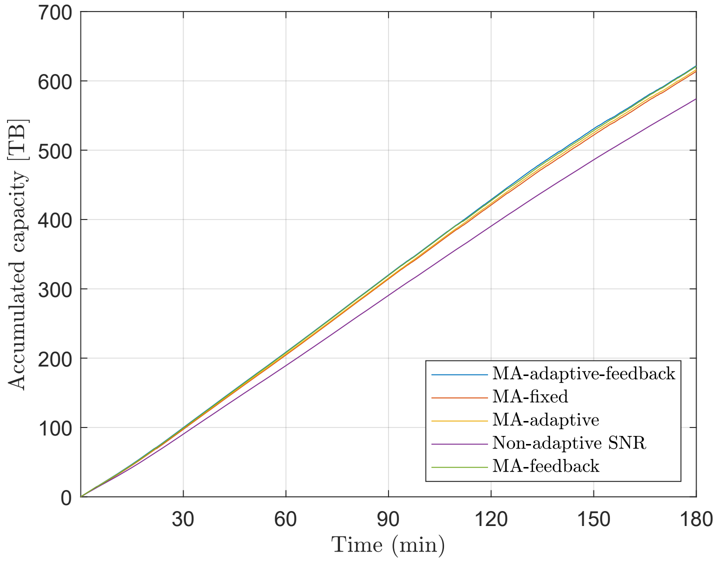

(b)

Figure 3.4: Accumulated capacity over time of every transmission for optimal (a) and non optimal (b) weather conditions

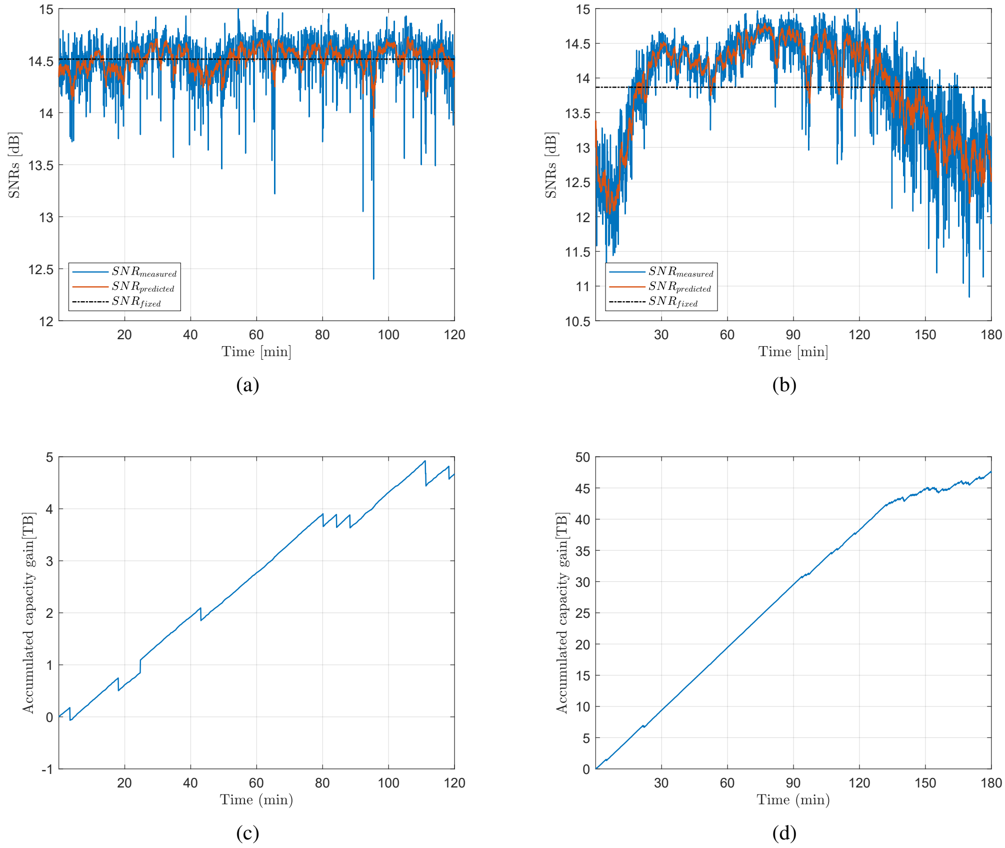

Figure 3.5: (a) and (b) : Emulated received SNR (in blue), respective MA-adaptive-feedback estimation (in red) and fixed-rate SNR(in yellow). (c) and (d):accumulated capacity gain of the adaptive transmission scheme vs the non-adaptive one for the respective (a) and (b) cases

3.3 Reliability

The importance of the $\text{SNR}_{\text{margin}}$ has been already widely discussed in the previous section but selecting different values can lead to different results in terms of reliability that are going to be showed in the following. Recalling the important role that FSO may assume in the future 5G scenario, its realiability is a key parameter to take it into account as an enabling technology for next generations. The Third Generation Partnership Project (3GPP) standard requires for the 5G wireless communication a reliability of at least 99.9999% to guarantee Ultra Reliable Low Latency Communication (URLLC). [26].

3.3.1 Expected results

It is clear that, the bigger the SNR margin, the better the reliability but a good tradeoff with the utilized channel capacity must be found. Again, the comparison is performed against a non adaptive transmission scheme. What's expected is that since the predictors are closer to the actual SNR value than its mean , the error among curves will be lower and the margin can be reduced when using a prediction scheme. The gap among the margins will be even higher in turbulent days as variations around the mean are higher.

3.3.2 Results

In Fig. 3.6 results are presented and the reliability is calculated as

$$\rho[\%] = 100 - \frac{N_{\text{NGMI}<\text{NGMI}_{\text{th}}}}{N} \tag{3.4}$$

where N is the total number of measurements and $N_{\text{NGMI}<\text{NGMI}_{\text{th}}}$ is the number of measurements in which the threshold NGMI has been violated. The SNR curves are the same as in Fig. 3.5, a) and b). The $\text{SNR}_{\text{margin}}$ tested ranges from 0.5 to 3.5 dB with a 0.1 dB granularity.

Table 3.1: Prediction scheme effect over the $\text{SNR}_{\text{margin}}$ to guarantee 100% reliability

	best margin non adaptive scheme	**best margin MA-adaptive-feedback**
2 hours sunny	2.2	1.6
3 hours rainy	3.1	1.7

It can be noticed first of all that the 5G requirement may be satisfied in using the proper $\text{SNR}_{\text{margin}}$, without losing too much in performance. As expected, the best margin to guarantee a reliable transmission is lower when using a prediction scheme with respect to a fixed one. Furthermore, the gap is increased in bad weather conditions and the gain in terms of accumulated capacity gain is furtherly increased as depicted in Fig. 3.7.

Of course, the price to pay to have a 100% reliable transmission is a reduction of the achievable mean bit rate caused by a higher needed margin; in fact , in perfect weather condition now in mean $R_{b,adaptive} = 460$ Gbps and $R_{b,non-adaptive} = 438$ Gbps and in rainy case $R_{b,adaptive} = 432$ Gbps and $R_{b,non-adaptive} = 380$ Gbps.

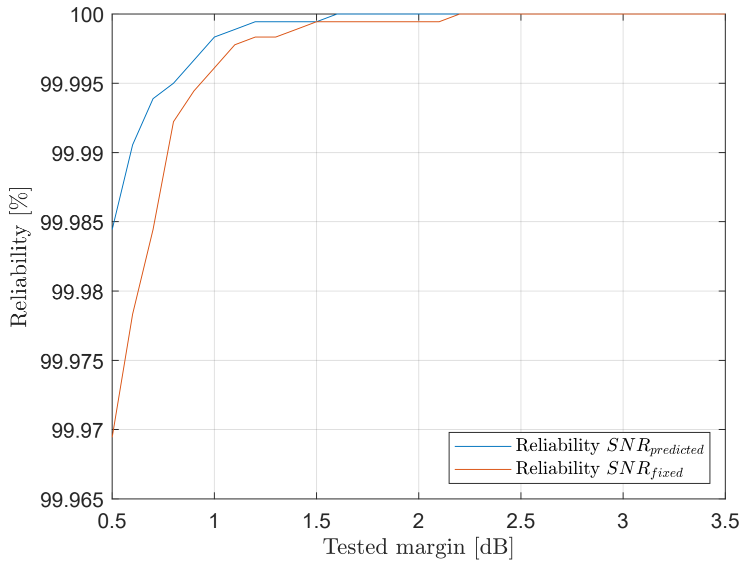

(a)

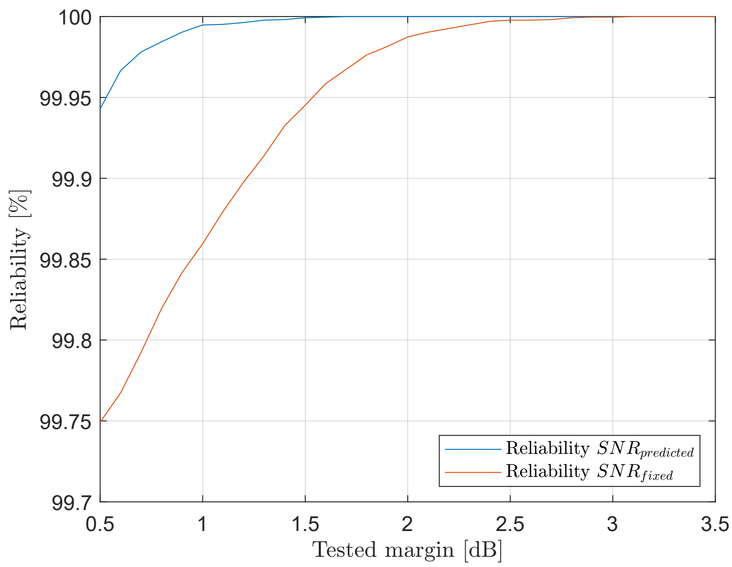

(b)

Figure 3.6: Reliability response as a function of different tested margins for sunny (a) and rainy (b) transmission cases

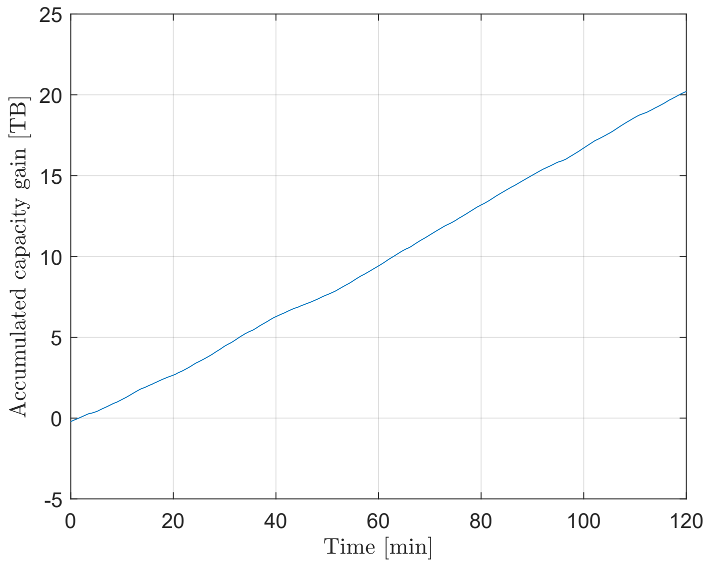

(a)

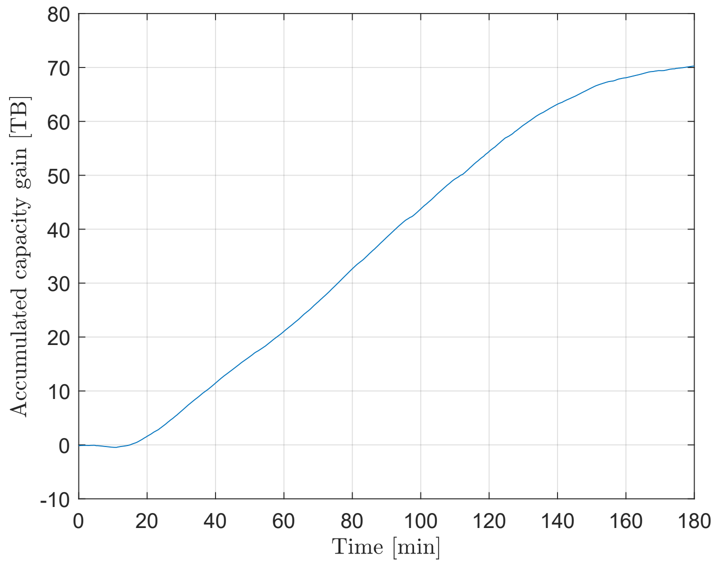

(b)

Figure 3.7: Accumulated capacity gain of an adaptive transmission scheme with respect to a non-adaptive one for a 100% reliable transmission in sunny (a) and rainy (b) cases

3.4 Sampling period

Another important result is about the sampling period of a FSO channel,i.e. how frequently the channel must be tracked in order to reliably set the transmission parameters and to have a low error prediction.

3.4.1 Expected results

In turbulent environmental conditions, in which the FSO channel is characterized by high variability, the sampling period must be lower in order to keep track of the variations while for stable weather conditions channel sampling can be less stringent.

3.4.2 Results

To evaluate different sampling periods, multiple of the original sampling period used for the power measurements $T_s = 4\mathrm{s}$ (From $2T_s$ (8 s) to $100T_s$ (>5 min)) are taken into account. To mimic this behavior, first the SNR curves are fitted with the MA-adaptive-feedback algorithm with a SNR_{margin} of $1\ \mathrm{dB}$, then, once every sample period, a value is sampled from the prediction vector and repeated as many times as the multiple of the sampling period. The result of this operation is presented in Fig. 3.8 for $10T_s$ and $100T_s$ both for sunny and rainy scenarios.

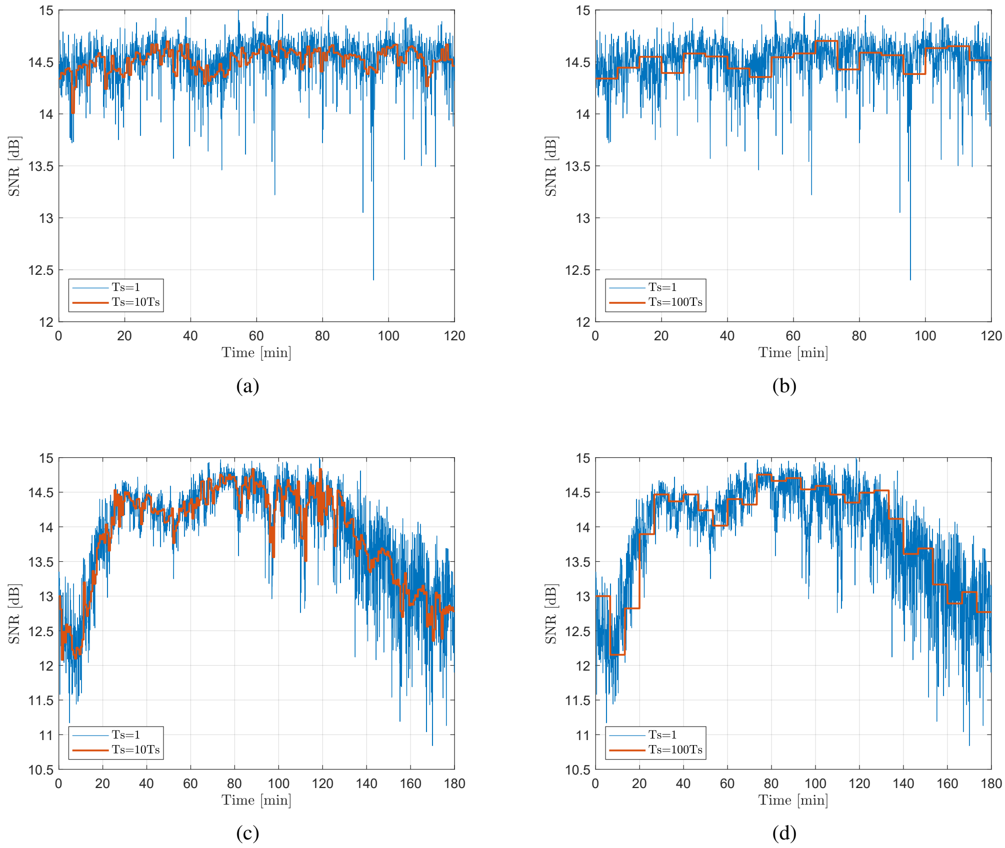

Figure 3.8: Different sampling periods effect for both weather profiles

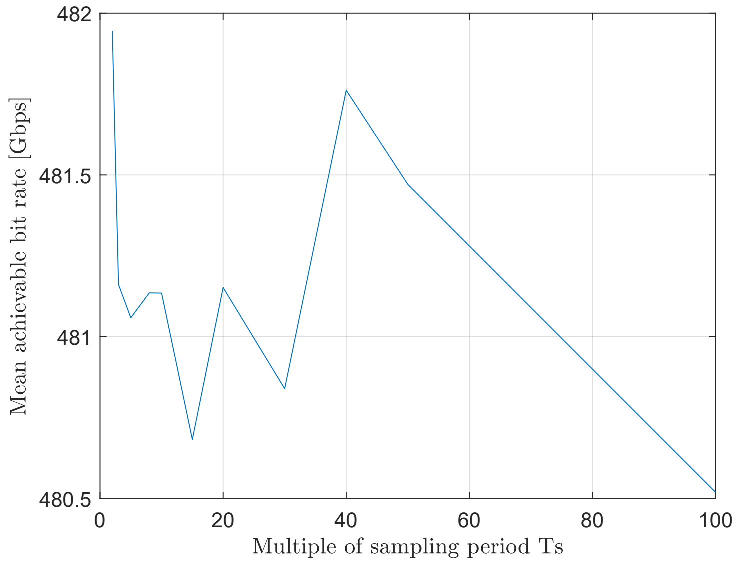

(a)

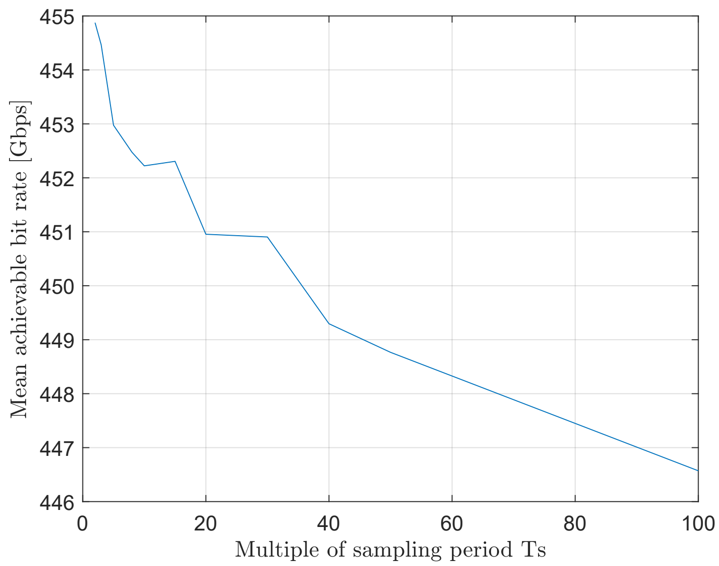

(b)

Figure 3.9: Mean achievable bit rate as a function of different tested sampling periods for sunny (a) and rainy (b) weather

A strange effect is obtained by plotting the achivable bit rate against the sampling period (Fig. 3.9). In rainy days, the bigger T_s the lower the mean achivable bit rate but the same can't be said for sunny days; in fact, the trend is not linear and this is justified by the fact that in good weather conditions the channel is characterized by random spikes around a stable mean. In those cases, whenever the channel is sampled, the sampling can be performed over a positive spike and channel overestimation will occur, or it can be performed on a negative spike and in that case there will be underestimation of the link. The behavior is thus totally random and because of that, in Fig. 3.10, a) by showing the capacity gain whenever considering a sampling period equal to $2\mathrm{T_s}$ against one equal to $100\mathrm{T_s}$, this randomness is noticeable in the quite low and unstable gain. On the contrary, for higher sampling periods, bad tracking is more likely to happen during turbulent environmental conditions and lose in capacity will occur as can be seen in Fig. 3.10, b).

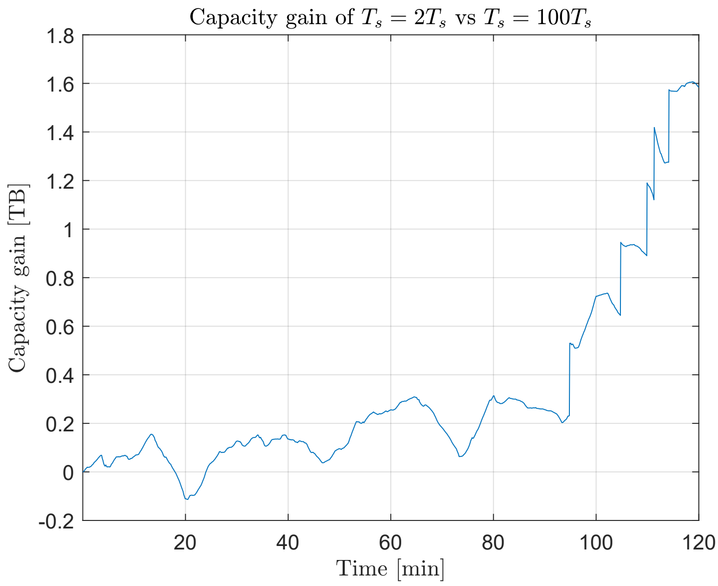

(a)

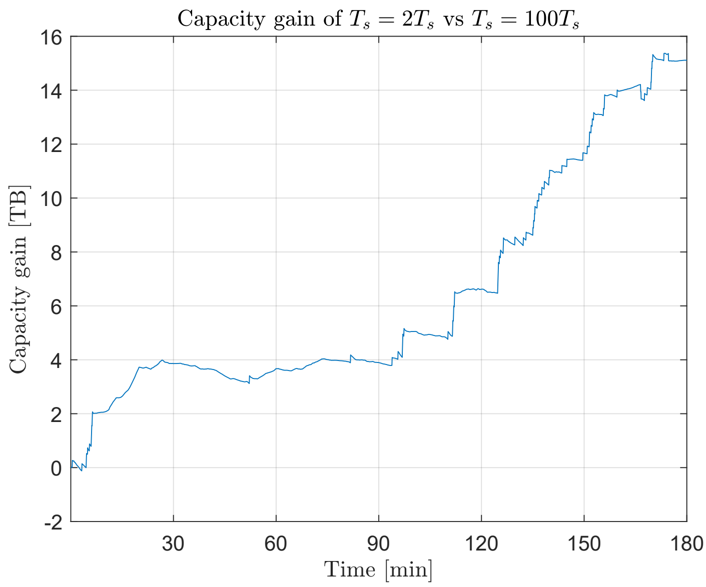

(b)

Figure 3.10: Accumulated capacity gain over time for sunny (a) and rainy (b) weather

3.5 Conclusions

The results first of all show in different ways the advantages, in terms of achievable rates and reliability, of using prediction algorithms able to know in advance channel conditions and set transmission parameters properly instead of doing it blindly, that is what happens for the non-adaptive transmissions cases. Furthermore, results provide a very interesting scenario that justifies the need to create channel profiles as suggested in chapter 2. In fact, what can be pointed out is that whenever the weather conditions are stable , a less stressed channel tracking can be performed, in terms of complexity of prediction algorithms, $\mathrm{SNR}_{\mathrm{margin}}$ values and sampling periods, without losing too much in capacity and reliability. On the other hand, in turbulent conditions, the better the prediction algorithm , the better the results in terms of capacity gain and reliability; of course, due to the high variability of the channel, its tracking must be more frequent and the $\mathrm{SNR}_{\mathrm{margin}}$ must be higher.

Since the weather conditions have this very important role, a joint work with meteorogical informations can lead to very interesting results. This will be further discussed in 5.2.1.

Chapter 4

High capacity system

To check the actual implementability of the proposed scheme, a laboratorial optical communication system is used. Now, a real modulated signal is transmitted continously through the FSO channel and batches of data are iteratively analyzed at the receiver front end in order to apply the prediction algorithm and perform the adaptive transmission.

4.1 Experimental setup

A list of the involved components is now listed and a scheme of the overall setup is provided in Fig. 4.1.

- **TRANSMITTER**
  - *External Cavity Laser (ECL)*
    - The optical source is a 100 KHz linewidth ECL. It transmits at 1550 nm and has an output power of +15 dBm.
  - *Digital Signal Processing (DSP)*
    - A CCDM is encharged of allowing a PCS transmission through a flexible bit rate by adapting symbol probability to the desired transmitted bit rate over a 64 QAM template. As in Chapter 3, the same parameters are set here for the transmitted signal so also in this case a maximum of 600 Gbps net bit-rate transmission can be achieved. In this case, the DSP pilots are QPSK-like symbols. The applied shaping pulse is a Raise Root Cosine (RRC) with a roll off $\rho = 0.05$.
  - *Arbitrary Waveform Generator (AWG)*
    - The baseband continous electrical waveform is generated and modulated at 64 Gbaud by an AWG operating at 120 Gsa/s, with 45 GHz of analog bandwidth.
  - *In phase and Quadrature (IQ) modulator*
    - The 22,5 GHz modulator gets in input the ECL and the output of the AWG in order to output a single polarization IQ modulated signal .
  - *Delay line (DL)*
    - In order to obtain two polarization, a frequently used technique is replicated for this scenario: the same signal from the output of the IQ modulator is splitted and one of the two branches is delayed by one meter that is enough to guarantee decorrelation between the tributaries. Before transmitting the signal through the channel, a manual polarization controller and a polarization beam splitter are used to optimize the transmitted power.

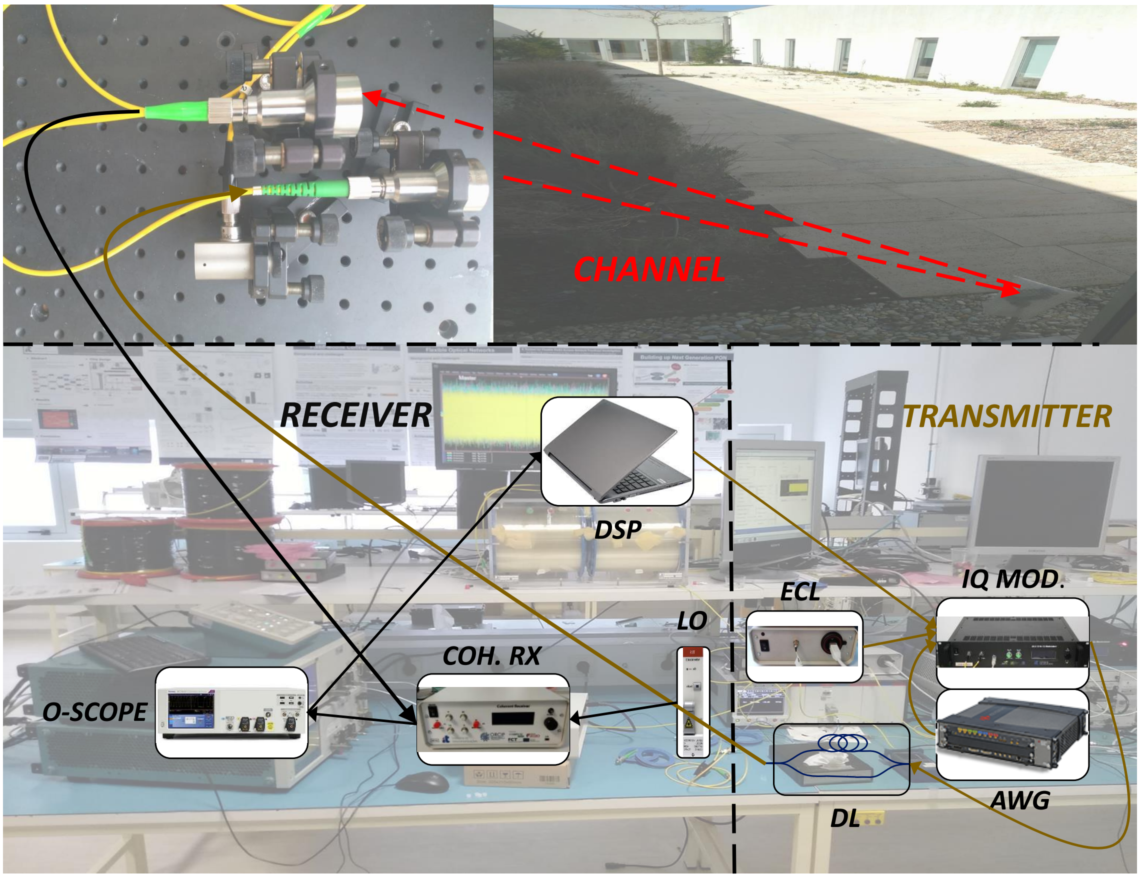

Figure 4.1: Experimental high capacity setup

- **FSO CHANNEL**
  - The FSO outdoor setup is the same used in Chapter 2, Fig. 2.1.
- **RECEIVER**
  - *Coherent receiver (COH. RX)*
    * A dual polarization 40 GHz bandwidth coherent receiver is used to downconvert the optical signal back to the electrical domain thanks to the mixing with a local oscillator signal. Signal is then sent to the oscilloscopes through four (one per polarization per component) phase-matched cables to avoid temporal delay between I and Q components.
  - *Local oscillator (LO)*
    * The signal of a local oscillator with 100 kHz linewidth and +13 dBm output power is used to feed the coherent receiver to create the beat pulse to allow a intradyne conversion method typical of coherent reception schemes.
  - *Oscilloscope (O-SCOPE)*
    * Both polarizations of the electrical signal in its I and Q components are then digitized by a 4-port real time 100 GSa/s oscilloscope with an analog bandwidth of 33 GHz through a sampling and quantization phase. The processed signal is then sent to a MATLAB script to apply digital signal processing to compensate for channel impairments.

– *DSP*

  * The DSP role in coherent reception is fundamental. It is encharged of re-aligning reference phase and polarization frames to the transmitted ones, compensate for chromatic dispersion, track frequency and phase shifts and perform matched filtering and clock recovery. Receiver frontend imbalance is compensated by a Gram-Schmidt orthogonalization procedure [27] and consequently by a DC component removal. After an initial training stage for convergence purposes, a pilot based first raw equalization and polarization demultiplexing is performed by a 25 taps in 2x2 butterfly fashion Constant Modulus Algorithm (CMA) based equalizer. Frequency recovery and carrier phase estimation is obtained by the QPSK pilot symbols. For fine tuning equalization and residual IQ skew a 51 taps 4x4 (for both polarizations in both I and Q components) Least-Mean Square (LMS) based equalizer is applied. Finally the signal is downsampled and demapped.

It's worth noting that one of the main advantages of a FSO setup is that it can mostly use the same components and follow the same rules of a fiber based transmission system, that is way more investigated. The main metrics to focus on are the NGMI and the SNR. NGMI is calculated following the procedure in [24] while the SNR is extracted from the Error-Vector Magnitude (EVM) between the demapped signal and the transmitted one through the relation : $\mathrm{SNR} = -20\log_{10}(\mathrm{EVM}_{\%}/100)$ where $\mathrm{EVM}_{\%} = \sqrt{\frac{\sum_{n=1}^{N}|y(n)-x(n)|^2}{\sum_{n=1}^{N}|x(n)|^2}} \cdot 100$, being x the transmitted signal and y the received one.

The results of a continuous three hours transmission are analyzed using the proposed system.

4.2 Results

A MATLAB routine is encharged of iteratively loading three signals for three different modulation schemes using PCS-64QAM : 1) a fixed modulation at 400 Gbps 2) a fixed modulation at 500 Gbps and 3) an adaptive modulation with bit rate adapted to the measured SNR.

The predicted SNR is obtained by means of the MA-fixed algorithm. This choice is justified by the fact that, since the weather conditions weren't good and, as showed in the previous chapter, the sampling frequency must be low to avoid erroneous prediction, and since by using a complete transmission setup a lot of time is required for signal loading and reception, the usage of the fastest algorithm was the most adequate choice. Numerically, every iteration took ~20s. Before conducting the actual measurements, thanks to a long term average behavior analysis of the FSO link in SNR terms, the best number of taps is found to be $N_{\mathrm{taps}} = 3$ with $\mathrm{SNR}_{\mathrm{margin}} = 2$ dB.

The adaptive modulation signal to be loaded is dictated by the AIR of the estimated SNR (SNR_{est}) whose formula is the 4.1; in fact, thanks to an already implemented function similar to the ones in section 3.1, the AIR can be easily extracted by considering, in this case, $M_{PCS} = 64$ and $NGMI_{th} = 0.9$.

$$SNR_{est}(n+1) = \frac{1}{3}\sum_{n-3+1}^{n} SNR_{measured} - SNR_{margin} \tag{4.1}$$

$$AIR(n+1) = f(SNR_{est}(n), NGMI_{th}, M_{PCS}) \tag{4.2}$$

During the 180 minutes measurement, for each iteration, a batch of $2 \cdot 10^5$ samples for the three modulation schemes is collected by the oscilloscope.

The measured SNR and its estimation are displayed in Fig. 4.2 and it can be noticed that even in this case a very simple algortithm is able to provide a very good estimation. The blue boxes on the image represent the rainy periods where it can be noticed that, as it was for the rainy power measurement of Fig. 2.10, the curve presents losses of almost 3 dB.

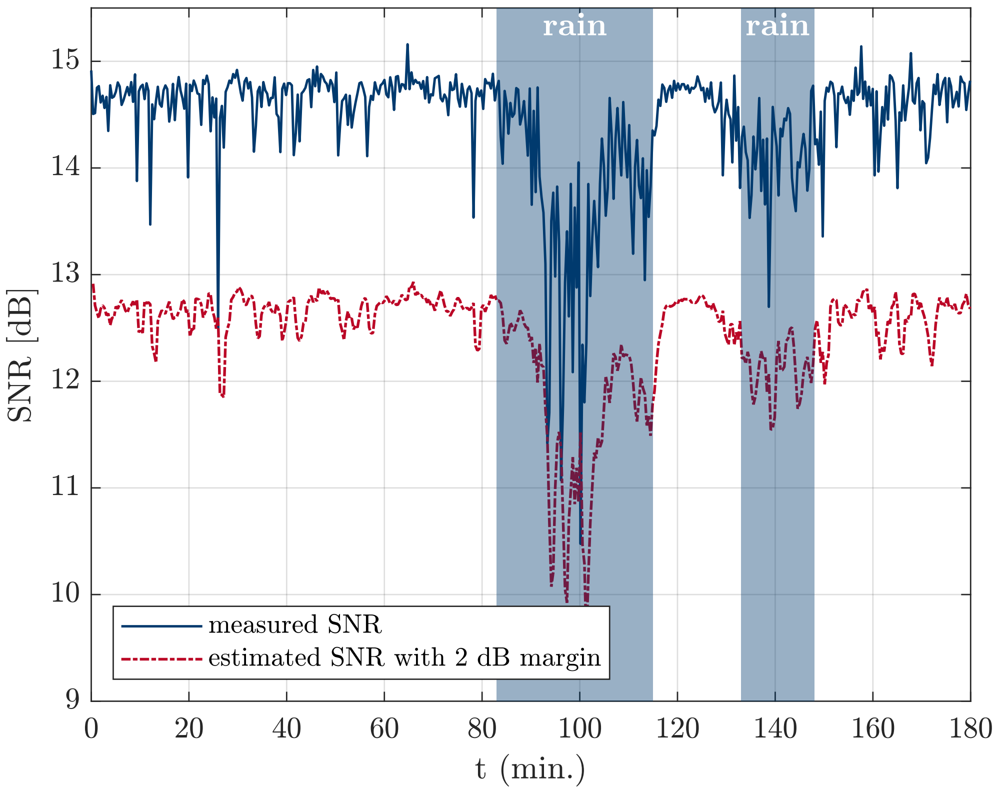

Figure 4.2: Time evolution of the measured SNR (in blue) and its estimation (in red)

By analyzing the NGMI plots in Fig. 4.3, a), the 500 Gbps NGMI presents many out of service periods, mostly during the rainy periods while, on the contrary, the 400 Gbps is able to survive also in those cases. This is exactly the same scenario presented in the previous chapter about the problems of over utilization or under utilization of the channel. In the 500 Gbps case the channel is too much exploited and, as soon as there is a sudden big variation in the mean, the signal is lost while on the other end the 400 Gbps case presents such a high margin that, even if the transmission is very reliable, the channel is not fully exploited as it can be seen by analyzing the mean value of the NGMI.

The NGMI curve related to the adaptive transmission (Fig. 4.3, b)), instead, presents a more stable value but closer to the $NGMI_{th}$ so that, especially during turbulent instants, variations are so high that even the predictor is not able to track it and even a 2 dB SNR_{margin} is not enough to compensate for those variations and signal is lost also in those cases. Anyway, it can be seen that the number of losses is way lower than for the 500 Gbps case.

The extraction of the bit rate R_b from the AIR is the same as in formula 3.1 . Instantaneous achievable bit rates are showed in Fig. 4.4, a), and even in this case, whenever an out-of-service transmission occurs (NGMI<0.9), the bit rate is considered to be 0. The average rate of the 400Gbps transmission over the 3 hours measurement is 399.8 Gbps, justifying its great resilience because of the high margin. For what concerns the 500Gbps transmission, during stable weather conditions it is able to sustain a very high speed communication, but whenever it has to face a turbulent scenario the link is down leading to an average rate of 426.6 Gbps. The adaptive one, on the other hand, thanks to its bit rate adaptability based on channel conditions, is able to provide an average bit-rate of 464 Gbps.

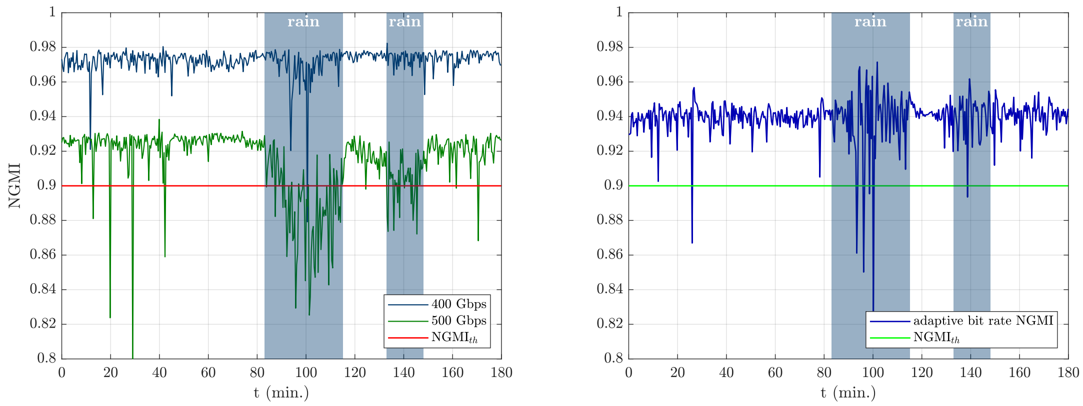

(a) (b)

Figure 4.3: NGMI evolution over time for a)fixed PCS-64QAM carring 400 Gbps and 500 Gbps and b)adaptive PCS

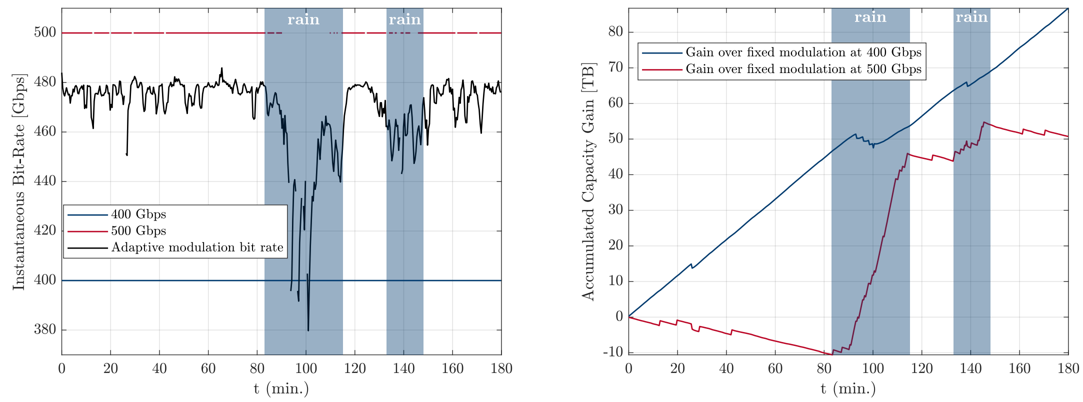

(a) (b)

Figure 4.4: a)Instantaneous achievable bit rate for fixed and adaptive modulation b)Accumulated capacity gain over time of the adaptive modulation with respect to the fixed ones

The last important result to show is related to the accumulated capacity gain over time of the adaptive scheme with respect to the two fixed bit rate transmissions. The gain over the 400 Gbps is basically constant over the full period of measurement, except for brief times during the heavy rainy periods, leading to an overall gain of >80 Terabytes. The gain over the 500 Gbps is negative during the calm weather period but it's largely compensated during the rainy periods leading to an overall gain of >50 Terabytes. Graphical results are displayed in Fig. 4.4, b).

4.3 System Enhancements

Some LUTs are built to enhance system performances in two ways: the first is related to the automatic gain of the coherent receiver and its impact over the signal reception. The other one has the goal of correlating the received power with post-processing SNR, since the latter is used to perform prediction following the strategy presented in the last section. This will bring benefits because: first, time is saved in processing and this will help in reducing the interval of time that passes from an iteration to another to let predictors better track channel variations. Then, it can simplify a lot the prediction method as it requires just the use of a power meter to load the next bit rate, which will be based on the outcome of the LUT instead of involving the whole receiver. Previously proposed scheme and its simplification are presented in Fig. 4.5.

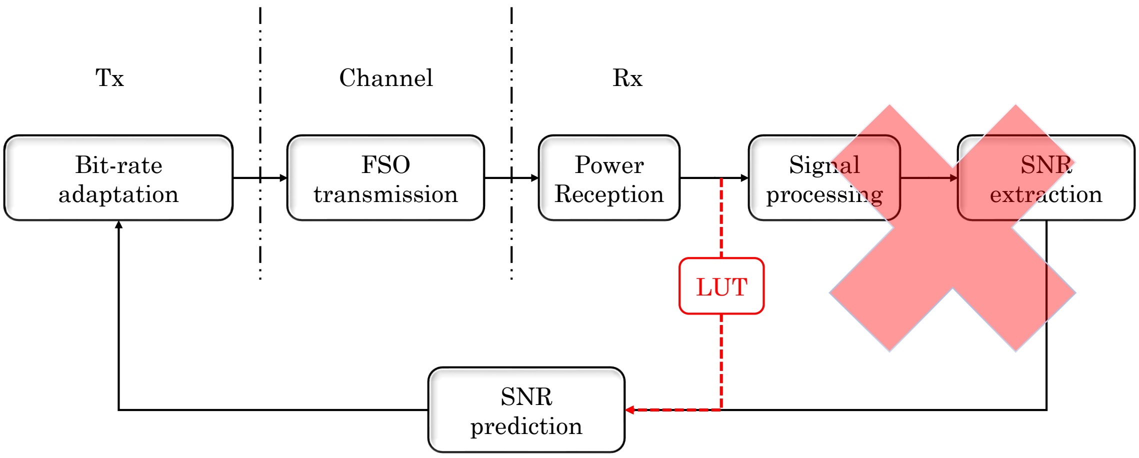

Figure 4.5: Simplification introduced by the LUT (in red) over the SNR extraction method in the previously used transmission scheme (in black)

The LUTs are built in the following way : A Variable Optical Attenuator (VOA) is now connected (instead of the FSO outdoor setup) and is set to provide attenuation values that range from 5 dB to 15 dB and the DSP is used to calculate the corresponding received SNR via the EVM method as in the previous section. These values are thought to take into account channel losses, interconnection cables and connectors to have the FSO-LAB connection and to also have some margin for turbulent situations. In the end, thanks to a 1:99 beam splitter placed immediately after the VOA, power variations can be tracked and for every tested attenuation a relation between power and SNR is found.

The automatic gain is an electronic amplifiers-based component that, whatever signal variation at its input, it will always try to maintain a stable amplitude at its output. By considering the setup of Fig. 4.1, the effect of applying an automatic gain on the coherent receiver is noticeble on the oscilloscope's vertical scale; in fact, whenever the received signal is set to be at the maximum scale of the oscilloscope, by increasing the attenuation, the automatic gain maintains the received curves over the full vertical scale resolution while when not using it, the full scale is not exploited resulting in a lower received SNR. A graphical demonstration is provided in Fig. 4.6 where a maximum attenuation of 15 dB is set on the VOA.

Two groups of LUTs are built, one taking into account the automatic gain of the coherent receiver and another one not taking it into account. In Fig. 4.7 the two groups for different bit rates are displayed. Powers are as low as -40 dBm because of the splitter.

These results show that using the automatic gain at the receiver side can lead to higher SNR for higher attenuations, thus higher performances but on the other end it may erase part of channel memory as fluctuations are reduced and predictors performances may be affected. That's the reason why previous results were obtained without the use of the automatic gain.

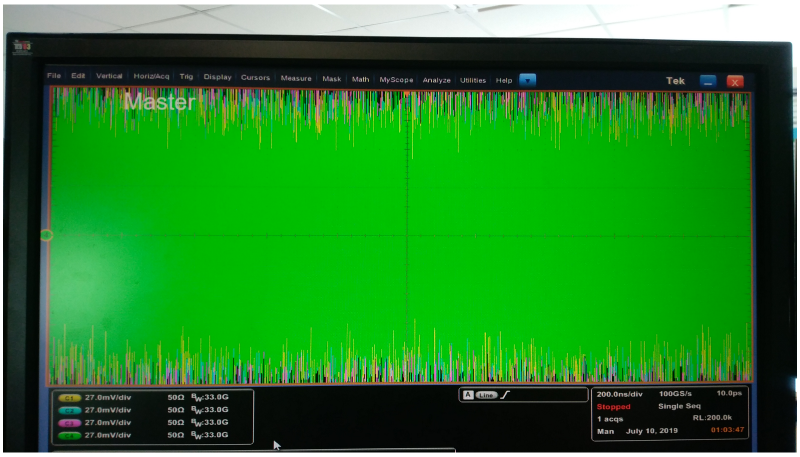

(a)

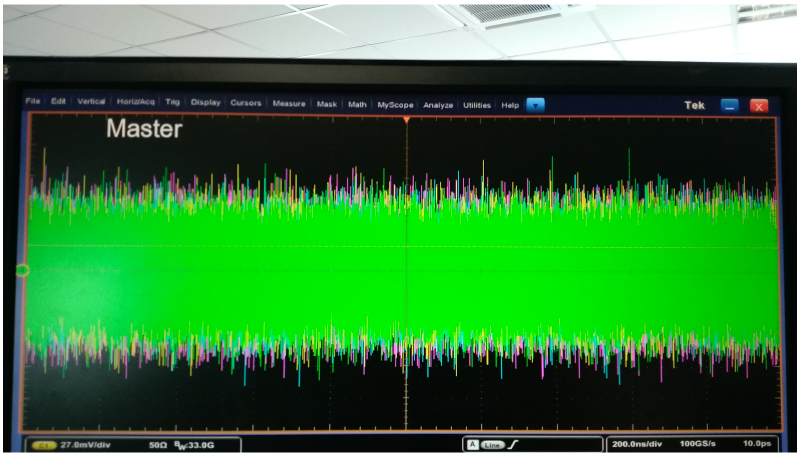

(b)

Figure 4.6: Automatic gain effect on the oscilloscope's vertical scale for the same attenuation a)Automatic gain enabled b)automatic gain disabled

For what concerns usability of the LUTs, an attenuation vector extracted from the rainy measurement of Fig. 2.10 is loaded to the VOA in order to have a wider range of attenuation values. Attenuation vector is displayed in Fig. 4.8 and at each iteration the VOA is loaded with a value from the vector.

It can be seen from Fig. 4.9 that the error among after-demapper-SNR and SNR-LUTs-based[1] curves is very low, thus LUTs approach can be considered as a good way to save time among iterations and have higher granularity in received SNR values that can be exploited by predictors to better track channel responses. Anyway, further validations are required and leaved as future work.

[1]A first test is made in order to check what is the achievable bit rate by considering the attenuation vector and only after a LUT for that specific bit rate is built. In this case a 470 Gbps LUT.

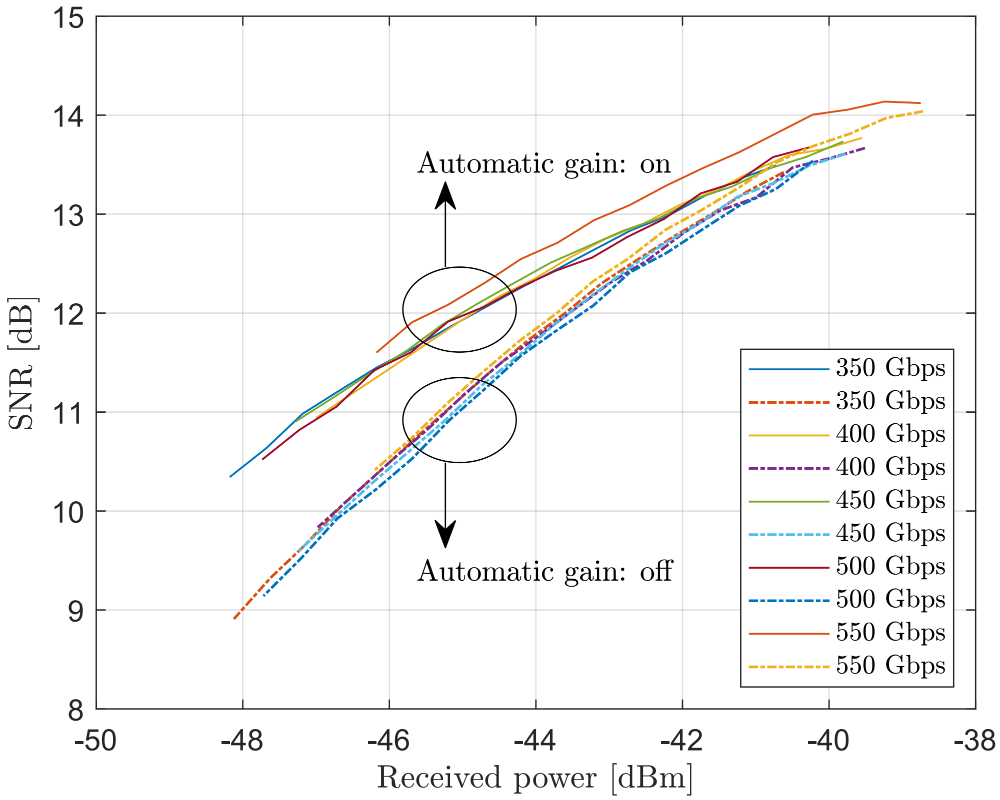

Figure 4.7: Outcome of LUTs for different tested bit rates, with and without the automatic gain enabled

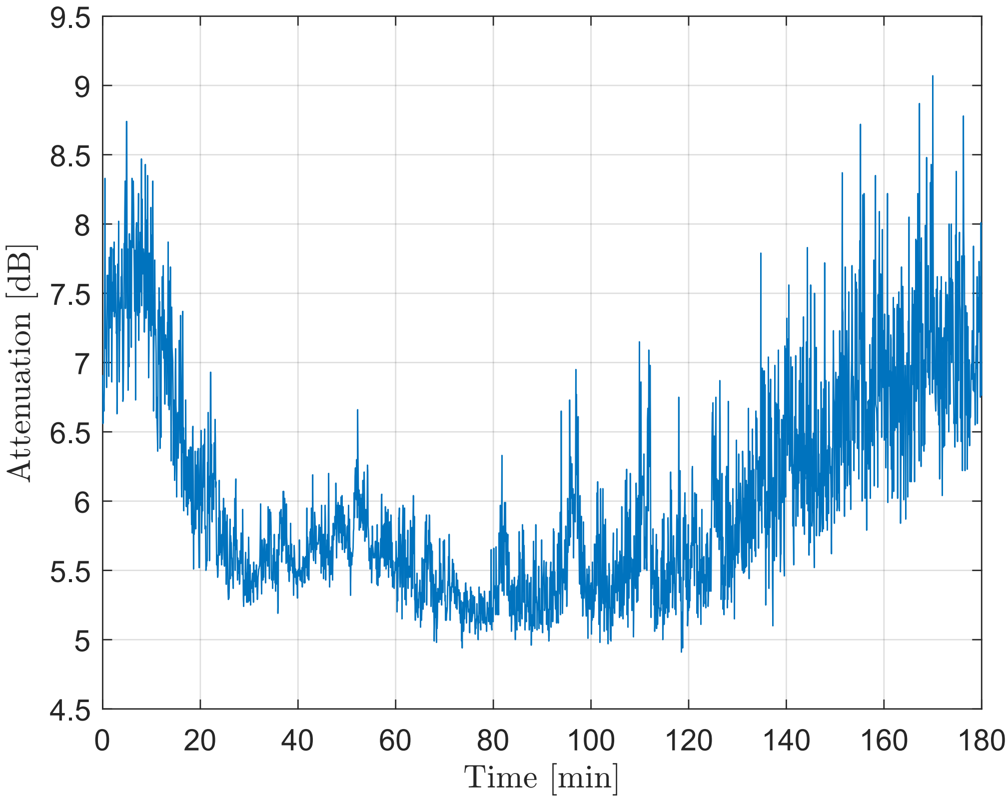

Figure 4.8: Attenuation vector provided to the VOA derived from Fig. 2.10, bottom

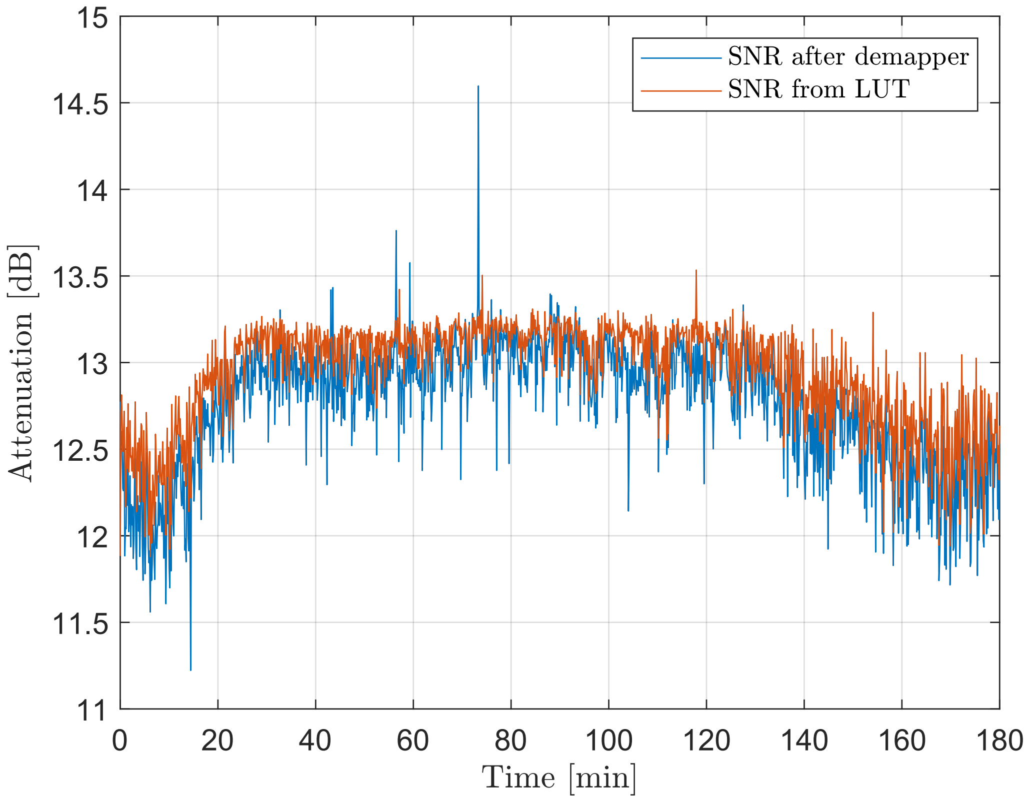

Figure 4.9: LUT's SNR fitting over the after-demapper-SNR

Chapter 5

Conclusions and future works

5.1 Conclusions

The first step to approach FSO was to collect power measurements from an outdoor setup. They were useful to understand FSO channel loss behavior and find the very interesting property of channel memory; in fact inter-dependency among collected samples was first noticed and then confirmed by an autocorrelation analysis of the acquired vectors. The channel memory is then exploited to build some moving-average-based predictors, whose working capability is then proved by a MSE in the order of 0.1 among real measurements and predictions.

During these experiments, by taking channel measurements in rainy days, the idea of making some profiles based on current weather status arised. This was proved to be very useful by analyzing the autocorrelation function and number of taps variation for an adaptive moving average filter that proved completely different results for rainy or sunny days.

Despite of these very good results, there was the need to test a complete transmission system introducing these new elements and check if they could bring some improvements.

A first offline processing phase was used to understand advantages and limits of the proposed algorithms. In order to do that, a 64-QAM PCS based simulated transmission was performed over the same power vectors converted into emulated received SNR values by simply adding a linear offset. Results showed all but gain of the adaptive transmission with respect to the non adaptive ones both in terms of performance (more achievable mean bit rates and accumulated capacity over time) and reliability (a lower SNR margin can be used when using a predictor). The need for channel profiling was then proved to be useful when considering FSO sampling period, leading to the need for lower sampling in presence of a turbulent weather scenario, otherwise even the predictors can be uneffective.

In the end a real time high capacity outdoor FSO transmission was performed and again the advantages were numerically analyzed showing a mean achievable transmission rate of 464 Gbps, even in presence of rain, and a gain of the adaptive scheme to be more than 50 and 80 TB for respectively an over provisioning fixed transmission scheme (500 Gbps) and an under provisioning one (400 Gbps).

These results showed how to maximally exploit FSO channel and at same time guarantee a reliable transmission thanks to the joint work of probabilistic constellation shaping and channel predictors. This scheme can be used as a starting point to develop high capacity FSO communication links in the future. Furthermore, a practical proof of FSO resistence to rain is provided. Last but not least, the simplicity of the proposed setup can further put VOA in the spotlight as a low cost solution for future wireless transmissions as well as enabling technology for next cellular generations.

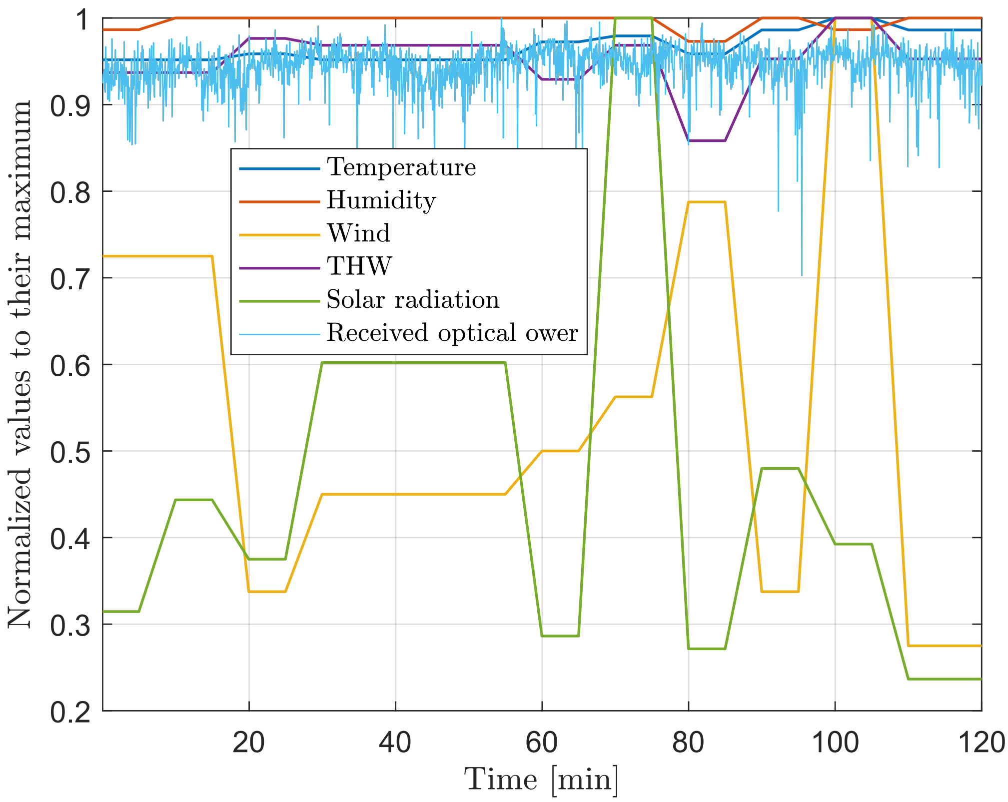

Figure 5.1: Example of weather forecast data integration with FSO power measurements

5.2 Future works

5.2.1 Weather forecast integration

Due to the big impact of the weather on an FSO communication and the related importance of channel profiling presented in this thesis, a future work that can be immediately addressed is about the role that a weather forecast can have on a FSO system. In fact, even if some considerations about attenuation can be done almost immediately, it can be interesting to see with what these variations are related to. To do so, a MATLAB script was implemented to connect to the University of Aveiro weather forecast site (`http://climetua.fis.ua.pt/weather`) and get real time data. The joint reception of power measurements and weather data from the Internet is shown in Fig. 5.1. Unfortunately, update rate of the meteorological data provided by the aforementioned website is rather slow (approximatively 5 minutes), which makes it difficult to find meaningful correlations with the optical power measurements in the medium term. Nevertheless, it could be worth running a longer-term experiment (several days) to exploit the correlation between weather conditions and FSO power budget.

This leaves an open door for future work and for sure, recalling their impact on sampling periods and $\mathrm{SNR}_{\mathrm{margin}}$ presented in chapter 3, weather conditions need to be known in advance to set the system in the proper way of working.

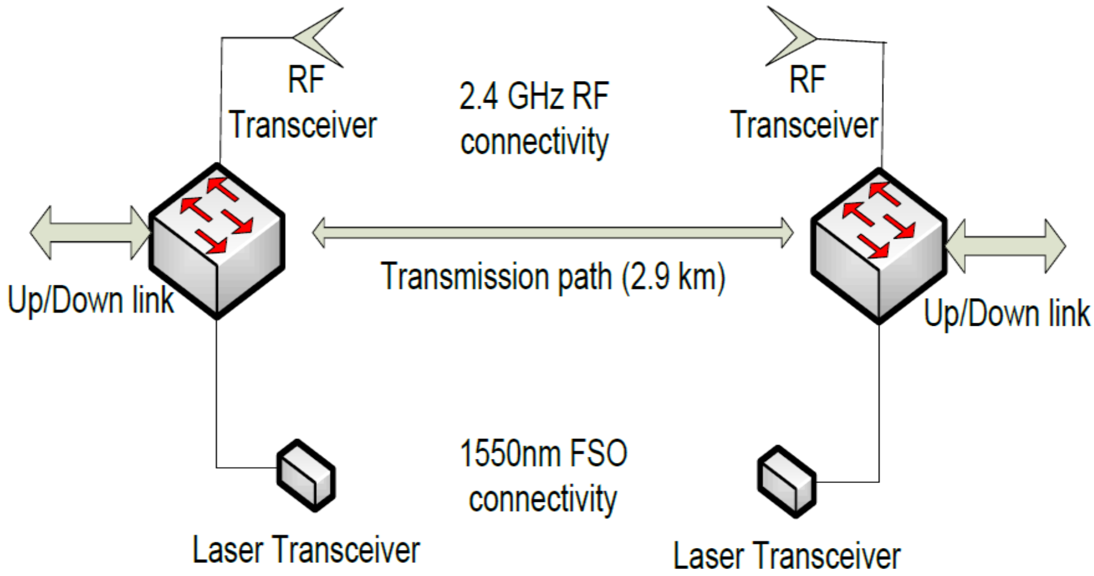

Figure 5.2: A possible hybrid RF/FSO architecture taken from [7]

5.2.2 Hybrid RF/FSO system

One of the main reasons to integrate RF systems with FSO is because of different responses to atmospheric impairments such as rain and fog; in fact, RF is more affected by rain than FSO but is more resilient to fog that, instead, is catastrophic for the latter. In systems like the one used in this thesis, which do not employ optical amplification and are based on a full LOS transmission, it is very important to maintain the link up and avoid any kind of obstruction of the optical beam. In these cases an RF backup system can help in both increasing link reliability as well as increasing the system capacity as it can be used as a recovery link (1+1 protection scheme) for dramatic atmosphere conditions (fog) or as a lower rate link (1:1). In Fig. 5.2 from [7] a backup system is suggested : RF and FSO both transmit data in parallel and whenever FSO signal crosses a lower bound threshold that may be based on the received signal quality, transmission switches entirely to RF. RF link can also be used to provide channel information to the transmitter. In this thesis' proposed system, this technique can be used to develop more precise predictors.

5.2.3 Pre-amplified FSO

As stated at the beginning, since EDFA work in the 1520-1600nm range, they are fully compatible with the setup proposed here because every transmission is driven by a 1550 nm laser. The use of EDFA-based FSO transmissions has been proposed as a good way to reduce the scintillation effect in the weak turbulence regime [28] but on the other end it can add Amplified Spontaneous Emission (ASE) degrading signal reception. Even if it would raise the costs and may have a strange impact on the proposed system and algorithms, as it may lower signal fluctuations at the receiver side and attenuate in part the inter-dependency among samples exploited by predictors, it is worth trying to further explore this path.

5.2.4 MIMO FSO

Another obliged way to either improve reliability or performance of an outdoor FSO system like the one studied in this thesis is by employing an array of transmitting and receiving optical collimators in the so called Multiple Input Multiple Output (MIMO). Apart from the huge advantages in terms of throughput that for sure a MIMO system offers, the main usage of multiple array system presented in literature is to mitigate turbulence induced fading effect thanks to channel diversity at the transmitter side [29]. Transmitter diversity means sending different signals on different beams to what is called repetition coding. Diversity can also be used at the receiver side by using multiple apertures at the receiver. In particular using several smaller apertures at the receiver, each one will benefit from some degree of aperture averaging that is a way to average intensity fluctuations of the received beam. The use of multiple apertures is more advantageous in the strong turbulence regime and is proved in [30]. Further validation can be achieved with the proposed setup, even if the strenght point of being a low cost system may suffer since a MIMO system is know to require more instrumentations and processing.

5.2.5 Automatic aligning system

A work made in parallel over the same used setup was about the installation of a motorized mirror, instead of the fixed one used in the setup of Fig. 2.1, to first blindly let the transmitter align to the Field-of-View (FOV) of the receiver and then keep track of the best position thanks to a feedback system in order to maximize the received power i.e. keep the FSO transmission. Acquisition, Tracking and Pointing (ATP) mechanisms are very useful for any kind of FSO system, from the long range ones to the one used for this thesis. ATP systems can help in lowering geometric losses, pointing errors and turbulence effects [31]. Pointing errors are one of the most experienced impairments during signal acquisitions along all the period of this study. It is defined as defined as the Euclidean distance between the centers of the receiver lens and the beam footprint at the receiver and as already pointed out in the introduction part, it may be caused by thermal expansion, building sway, mechanical stresses and atmospherical adverses conditions. All these type of problems were faced also by the studied system. In literature many other ATP mechanism are proposed, including adaptive optics, gimbal and rotating head [31]. Automatic aligning may be useful to reduce signal variance and consequently let the proposed prediction algorithms be less erroneous.

5.2.6 Neural network assistence

Machine learning algorithms to optimize FSO communications are recently gaining more and more attention [32]. With a huge dataset of power measurements it would be possible to create some training networks, maybe one per channel profile, in order to create some fitters able to predict channel response in a very precise way, potentially enabling higher-precision SNR estimation.

Bibliography

[1] A. G. Bell. “Upon the production and reproduction of sound by light”. In: *Journal of the Society of Telegraph Engineers* 9.34 (1880), pp. 404–426. DOI: 10.1049/jste-1.1880.0046.

[2] CISCO White paper. *Cisco Visual Networking Index : Forecast and Trends ,2017-2022*. 2019.

[3] International Data Corporation. 2015. URL: https://www.idc.com/.

[4] Mohamed Alzenad et al. “FSO-Based Vertical Backhaul/Fronthaul Framework for 5G+ Wireless Networks”. In: *IEEE Communications Magazine* 56.1 (2018), pp. 218–224. ISSN: 01636804. DOI: 10.1109/MCOM.2017.1600735.

[5] Mohammad Ali Khalighi and Murat Uysal. “Survey on free space optical communication: A communication theory perspective”. In: *IEEE Communications Surveys and Tutorials* 16.4 (2014), pp. 2231–2258. ISSN: 1553877X. DOI: 10.1109/COMST.2014.2329501.

[6] Marzieh Najafi and Vahid Jamali. “C-RAN with Hybrid RF / FSO Fronthaul Links : Joint Optimization of RF Time Allocation and Fronthaul Compression”. In: December (2017). DOI: 10.1109/GLOCOM.2017.8254767. arXiv: arXiv:1808.05004v1.

[7] Rayan A. Alsemmeari, Sheikh Tahir Bakhsh, and Hani Alsemmeari. “Free Space Optics Vs Radio Frequency Wireless Communication”. In: *International Journal of Information Technology and Computer Science* 8.9 (2016), pp. 1–8. ISSN: 20749007. DOI: 10.5815/ijitcs.2016.09.01.

[8] Abdelbaset S Hamza, Jitender S Deogun, and Dennis R Alexander. “Classification Framework for Free Space Optical Communication Links and Systems”. In: *IEEE Communications Surveys & Tutorials* 21.2 (2019), pp. 1346–1382. DOI: 10.1109/COMST.2018.2876805.

[9] Isiaka Alimi et al. “Challenges and Opportunities of Optical Wireless Communication Technologies”. In: *Optical Communication Technology*. 2017. DOI: 10.5772/intechopen.69113.

[10] Scott Bloom, Eric Korevaar, and John Schuster. “Understanding the performance of free-space optics [Invited]”. In: 2.6 (2003), pp. 178–200.

[11] Michael Unser et al. “Performance Evaluation of Free Space Optics (FSO) and Radio Frequency Communication System Due to Combined Effect of Fog and Snow”. In: *2015 37th Annual International Conference of the IEEE Engineering in Medicine and Biology Society (EMBC)* 50.3 (2002), pp. 728–737. ISSN: 0277786X. DOI: 10.1117/12.595149. arXiv: 1507.00136.

[12] A. Vavoulas, H. G. Sandalidis, and D. Varoutas. “Weather effects on FSO network connectivity”. In: *IEEE/OSA Journal of Optical Communications and Networking* 4.10 (Oct. 2012), pp. 734–740. DOI: 10.1364/JOCN.4.000734.

[13] X. Liu. “Free-space optics optimization models for building sway and atmospheric interference using variable wavelength”. In: *IEEE Transactions on Communications* 57.2 (Feb. 2009), pp. 492–498. DOI: 10.1109/TCOMM.2009.02.070089.

[14] Vladimir Sidorovich. “Solar background effects in wireless optical communications”. In: 4873 (Oct. 2002). DOI: 10.1117/12.456303.

[15] G. Forney et al. “Efficient Modulation for Band-Limited Channels”. In: *IEEE Journal on Selected Areas in Communications* 2.5 (Sept. 1984), pp. 632–647. DOI: `10.1109/JSAC.1984.1146101`.

[16] Georg Böcherer, Patrick Schulte, and Fabian Steiner. “High Throughput Probabilistic Shaping with Product Distribution Matching”. In: (2017), pp. 1–9. arXiv: `1702.07510`. URL: `http://arxiv.org/abs/1702.07510`.

[17] Junho Cho and Peter J. Winzer. “Probabilistic Constellation Shaping for Optical Fiber Communications”. In: *Journal of Lightwave Technology* 37.6 (2019), pp. 1590–1607. ISSN: 07338724. DOI: `10.1109/JLT.2019.2898855`.

[18] Technical University of Munich. “"Optical fiber transmits one terabit per second"”. In: (Sept. 2016).

[19] Georg Bocherer, Patrick Schulte, and Fabian Steiner. “Probabilistic shaping and forward error correction for fiber-optic communication systems”. In: *Journal of Lightwave Technology* 37.2 (2019), pp. 230–244. ISSN: 07338724. DOI: `10.1109/JLT.2019.2895770`.

[20] P. Schulte and G. Böcherer. “Constant Composition Distribution Matching”. In: *IEEE Transactions on Information Theory* 62.1 (Jan. 2016), pp. 430–434. DOI: `10.1109/TIT.2015.2499181`.

[21] Dario Pilori et al. “Comparison of Probabilistically Shaped 64QAM with Lower Cardinality Uniform Constellations in Long-Haul Optical Systems”. In: *Journal of Lightwave Technology* 36.2 (2018), pp. 501–509. ISSN: 07338724. DOI: `10.1109/JLT.2017.2752842`.

[22] Fred Buchali et al. “Rate Adaptation and Reach Increase by Probabilistically Shaped 64-QAM : An Experimental Demonstration”. In: 34.7 (2016), pp. 1599–1609.

[23] Abel Lorences-Riesgo et al. “200 Gbit/s Free-Space Optics Transmission Using a Kramers-Kronig Receiver”. In: (2019), W4A.3. DOI: `10.1364/ofc.2019.w4a.3`.

[24] Junho Cho et al. “Normalized Generalized Mutual Information as a Forward Error Correction Threshold for Probabilistically Shaped QAM”. In: 8.1 (2017), pp. 17–19.

[25] A. Alvarado et al. “Achievable Information Rates for Fiber Optics: Applications and Computations”. In: *Journal of Lightwave Technology* 36.2 (Jan. 2018), pp. 424–439. DOI: `10.1109/JLT.2017.2786351`.

[26] Next Generation Mobile Networks (NGMN) alliance. “NGMN 5G WHITE PAPER”. In: (Feb. 2015).

[27] I. Fatadin, S. J. Savory, and D. Ives. “Compensation of Quadrature Imbalance in an Optical QPSK Coherent Receiver”. In: *IEEE Photonics Technology Letters* 20.20 (Oct. 2008), pp. 1733–1735. DOI: `10.1109/LPT.2008.2004630`.

[28] M. Razavi and J. H. Shapiro. “Wireless optical communications via diversity reception and optical preamplification”. In: *IEEE Transactions on Wireless Communications* 4.3 (May 2005), pp. 975–983. DOI: `10.1109/TWC.2005.847102`.

[29] Ahmed A Farid, Steve Hranilovic, and Senior Member. “Diversity Gain and Outage Probability for MIMO Free-Space Optical Links with Misalignment”. In: 60.2 (2012), pp. 479–487.

[30] M. Khalighi et al. “Fading Reduction by Aperture Averaging and Spatial Diversity in Optical Wireless Systems”. In: *IEEE/OSA Journal of Optical Communications and Networking* 1.6 (Nov. 2009), pp. 580–593. DOI: `10.1364/JOCN.1.000580`.

[31] Y. Kaymak et al. “A Survey on Acquisition, Tracking, and Pointing Mechanisms for Mobile Free-Space Optical Communications”. In: *IEEE Communications Surveys Tutorials* 20.2 (2018), pp. 1104–1123. DOI: `10.1109/COMST.2018.2804323`.

[32] Laialy Darwesh and Shlomi Arnon. “Deep learning for free space optics in a data center environment”. In: Sept. 2018, p. 4. DOI: `10.1117/12.2321025`.